NASA CONTRACTOR REPORT

NASA CR-2397

NASA CR-2397

THE RADIATION FROM SLOTS IN TRUNCATED DIELECTRIC-COVERED SURFACES

by Y. M. Hwang, R. G. Kouyoumjian, and P. H. Pathak

Prepared by
THE OHIO STATE UNIVERSITY
ELECTROSCIENCE LABORATORY
Columbus, Ohio 43212
for Langley Research Center

NATIONAL AERONAUTICS AND SPACE ADMINISTRATION • WASHINGTON, D. C. • JUNE 1974

1. Report No.	2. Government Accession No.	3. Recipient's Catalog No.
NASA CR-2397		

4. Title and Subtitle	5. Report Date
THE RADIATION FROM SLOTS IN TRUNCATED DIELECTRIC-COVERED SURFACES	June 1974
	6. Performing Organization Code

7. Author(s)	8. Performing Organization Report No.
Y. M. Hwang, R. G. Kouyoumjian, and P. H. Pathak	TR 3001-8
	10. Work Unit No. 502-33-13-02

9. Performing Organization Name and Address	11. Contract or Grant No.
The Ohio State University ElectroScience Laboratory Columbus, Ohio 43212	NGR 36-008-144
	13. Type of Report and Period Covered
12. Sponsoring Agency Name and Address	Contractor Report
National Aeronautics and Space Administration Washington, D.C. 20546	14. Sponsoring Agency Code

15. Supplementary Notes

Topical report.

16. Abstract

A theoretical approach based on the geometrical theory of diffraction is used to study the electromagnetic radiation from a narrow slot in a dielectric-covered perfectly-conducting surface terminated at an edge. The total far-zone field is composed of a geometrical optics field and a diffracted field. The geometrical optics field is the direct radiation from the slot to the field point. The slot also generates surface waves which are incident at the termination of the dielectric cover, where singly-diffracted rays and reflected surface waves are excited. The diffraction and reflection coefficients are obtained from the canonical problem of the diffraction of a surface wave by a right-angle wedge where the dielectric-covered surface is approximated by an impedance surface. This approximation is satisfactory for a very thin cover; however, the radiation from its vertical and faces cannot be neglected in treating the thicker dielectric cover. This is taken into account by using a Kirchhoff-type approximation, which contributes a second term to the diffraction coefficient previously obtained. The contributions from the geometrical optics field, the singly-diffracted rays and all significant multiply-diffracted rays are summed to give the total radiation. Calculated and measured patterns are found to be in good agreement

17. Key Words (Suggested by Author(s))	18. Distribution Statement
Antennas, Spacecraft and Aircraft Antennas Applied Electromagnetic Theory	Unclassified - Unlimited STAR Category 09

19. Security Classif. (of this report)	20. Security Classif. (of this page)	21. No. of Pages	22. Price*
Unclassified	Unclassified	41	$3.25

*For sale by the National Technical Information Service, Springfield, Virginia 22151

Page Intentionally Left Blank

TABLE OF CONTENTS

I. INTRODUCTION

The purpose of this study is to examine the effectiveness of the geometrical theory of diffraction (GTD) in calculating the radiation from slots in perfectly-conducting surfaces which are partially covered with dielectric. Configurations of this type are of interest in the design of antenna systems for spacecraft. We consider the radiation from a narrow slot in a dielectric-covered perfectly-conducting surface terminated at an edge as shown in Fig. 1. This is

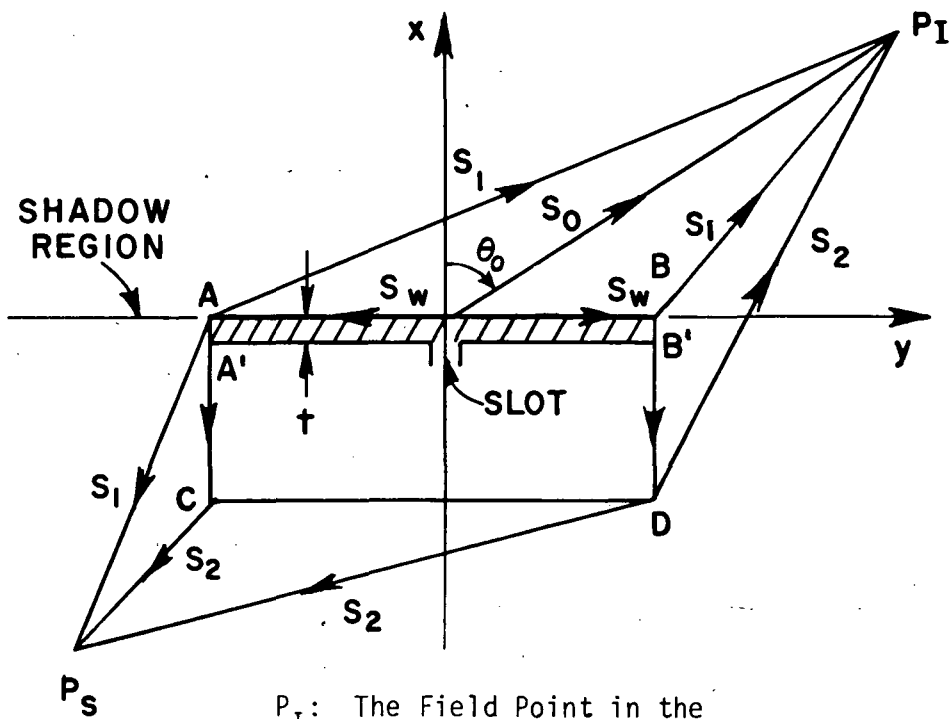

P_I: The Field Point in the Illuminated Region

P_S: The Field Point in the Shadow Region

S_0: Geometrical Optics Ray

S_1: Singly-diffracted Ray

S_2: Doubly-diffracted Ray

S_w: Surface Ray Traveling Parallel to the Dielectric Sheet

Fig. 1

one of the most elementary structures involving dielectric-covered slots; furthermore, measured patterns are available to check the GTD analysis [1].

A theoretical approach to the problem based on the geometrical theory of diffraction [2] is described. The effect of the truncation of the dielectric cover has been ignored in previous analysis, yet this yields the diffracted ray which plays a dominant role in determining the radiation pattern. The total far-zone field is composed of a geometrical optics field and a diffracted field. The geometrical optics field is the direct radiation from the slot to the field point P; it vanishes in the shadow region below the plane containing the surface AB. The slot also excites surface waves which are incident at the termination of the dielectric cover at A and B. The terminations yield singly-diffracted rays and reflected surface waves. For simplicity the thickness t of the dielectric cover is restricted so that only the dominant TM_0 surface wave mode is excited. The contributions from the geometrical optics ray, the singly-diffracted rays and all significant multiply-diffracted rays are summed to give the field at P.

The geometrical optics field and the field of the incident surface wave are obtained from the solution to the problem of a narrow slot radiating through a dielectric-covered ground plane of infinite extent. The diffraction coefficient and reflection coefficient for the surface wave incident on the edge A (or B) are determined in the following way. The surface impedance of the grounded, dielectric cover

$$(1) \qquad Z_s = Z_0 \frac{k_n}{k_0}$$

where k_0 and Z_0 are the wave number and characteristic impedance of free space, and k_n, which is found from the solution of a transcendental equation, is the wave number of the surface wave in the direction normal to the dielectric-covered surface (k_n is imaginary for a lossless dielectric cover). Next, consider a right-angle wedge, one of whose faces is perfectly-conducting, the other with surface impedance Z_s. The canonical problem of the diffraction of a surface wave by this right-angle wedge [3] is used to find diffraction and reflection coefficients, which are adequate for sufficiently thin dielectric covers. However, as the thickness of the cover increases, the radiation from the vertical end face AA' (or BB') of the dielectric cover cannot be neglected. This is taken into account using a Kirchhoff-type approximation, where the total electric field within the dielectric cover at its end face radiates in the presence of a right-angle wedge. This contributes a second term to the diffraction coefficient previously obtained.

The calculated and measured patterns compare well, which justifies the use of the geometrical theory of diffraction in this type of problem together with the approximations which have been used to find the diffraction coefficient. The patterns are very sensitive functions of the parameters, such as the thickness of the dielectric cover and the frequency. When the dielectric cover is lossy, the contributions from the diffracted rays decrease as the loss tangent of the dielectric cover increases. This is due to the fact that the surface wave is attenuated as it is incident at the termination of the dielectric cover. The ripples in the patterns in the illuminated region diminish and the level of radiation in the shadow region is reduced.

II. METHOD OF ANALYSIS

According to the geometrical theory of diffraction, the total far-zone field is composed of a geometrical optics field and a diffracted field. In the problem of a narrow slot in a dielectric-covered perfectly-conducting surface terminated at an edge (see Fig. 1), the geometrical optics field is the direct radiation from the slot to the field point; it vanishes in the shadow region. The singly-diffracted field is the field diffracted by the termination of the dielectric cover at A (or B). The termination of the ground plane at C (or D) yields a doubly-diffracted ray. In this chapter, the contribution from each ray will be described in detail.

A. The Geometrical Optics Field and the Field of the Surface Wave

Consider a magnetic line source on an infinite, perfectly-conducting ground plane covered by a dielectric slab of uniform thickness as shown in Fig. 2.

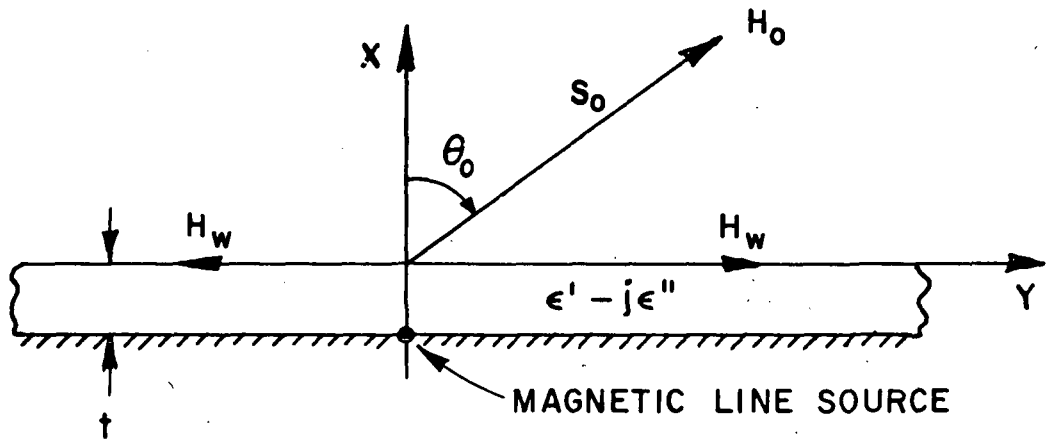

Fig. 2.

This configuration simulates the behavior of a narrow slot radiating through a dielectric cover. It is known that the line source excites a surface wave which propagates along the dielectric slab. It is a straightforward exercise to show that the geometrical optics field H_0 and the field of the surface wave due to a magnetic line source of unit strength are

$$(2) \qquad H_0 = -\frac{\omega\varepsilon_0\varepsilon_r \cos\theta_0}{\varepsilon_r \cos\theta_0 \cos\zeta_0 t + j\sqrt{\varepsilon_r - \sin^2\theta_0}\sin\zeta_0 t}\,\frac{e^{-j(ks_0 - \frac{\pi}{4})}}{\sqrt{2\pi k_0 s_0}}$$

$$(3) \qquad H_w = -\frac{\omega\varepsilon_0\varepsilon_r^2 \lambda^2 \zeta_w}{\beta \sin\zeta_w t[\varepsilon_r k_0^2(\varepsilon_r - 1) + \lambda t(\lambda^2\varepsilon_r^2 + \zeta_w^2)]}\,e^{-\lambda x - j\beta|y|}$$

where $\varepsilon_r = (\varepsilon' - j\varepsilon'')/\varepsilon_0$, the relative dielectric constant of the cover

k_0 is the free space wave number, $k = k_0\sqrt{\varepsilon_r}$

$\zeta_0 = k_0\sqrt{\varepsilon_r - \sin^2\theta_0}$

$$(4) \qquad \beta = \sqrt{k^2 - \zeta_w^2}$$

$$(5) \qquad \lambda = \sqrt{\beta^2 - k_0^2} \quad , \quad k_n = j\lambda \quad .$$

The value of ζ_w is determined from the transcendental equation

$$(6) \qquad \tan\zeta_w t = \varepsilon_r \sqrt{\frac{(\varepsilon_r - 1)(k_0 t)^2}{(\zeta_w t)^2} - 1} \quad .$$

In the case where the dielectric slab is lossy, ε_r and k are complex, and the root of Eq. (6) is complex. A method for calculating the complex root of a transcendental equation is described in Appendix 2. It is seen from Eqs. (4) and (5) that the important parameters of the surface wave β and λ are complex, so that the surface wave attenuates as it propagates.

Throughout this report a time dependence of $e^{j\omega t}$ is assumed and suppressed.

B. The Field of the Diffracted Rays

As noted in the preceding section, the slot excites a surface wave which propagates along the dielectric cover (slab). This surface wave is diffracted and reflected at the corners A, B shown in Fig. 1, so we seek the diffraction and reflection coefficients from the canonical problem of the surface wave incident on a dielectric-covered perfectly-conducting right-angle bend as shown in Fig. 3a. Since an exact solution to this problem is not available, we will replace it by an approximate canonical problem, which will be solved in two stages.

In the approximate canonical problem, shown in Fig. 3b, the dielectric slab is replaced by the impedance surface described by Eq. (1), with k_η given by Eq. (5). If this impedance boundary is positioned at the top surface of the cover, the field of the surface wave external to the cover is unaffected; however, it is apparent that the field within the cover is neglected. Thus one would expect the approximation to be good only when the ratio K of the power in the surface wave field external to the cover to the power within the cover is large. It can be shown that

$$(7) \qquad K = \frac{\varepsilon_r k_x \cos^2 k_x t}{\lambda(k_x t + \tfrac{1}{2}\sin^2 k_x t)} \,,$$

$$k_x = \sqrt{k^2 - \beta^2} \,.$$

It is seen that as t decreases, the ratio increases; and so the approximate canonical problem of Fig. 3b is useful only for thin dielectric slabs. The behavior of K as a function of the thickness t of the slab is shown in Fig. 4, for $\varepsilon_r = 2.56$.

Chu et al [3] have solved the problem shown in Fig. 3b; they give expressions for the far-zone diffracted magnetic field and the field of the surface wave reflected at the edge. Their diffracted field is

$$(8) \qquad H_{11} = -H_w \frac{A \cos\frac{\theta}{3}}{\lambda + jk_0 \cos\theta}\sqrt{\frac{2}{\pi k_0}}\, e^{j\frac{5\pi}{12}} \frac{e^{-jk_0 s_1}}{\sqrt{s_1}} \,.$$

According to the GTD,

$$(9) \qquad H_{11} = H_w D_{11} \frac{e^{-jk_0 s_1}}{\sqrt{s_1}} \,,$$

in which H_w is the surface wave field at the edge

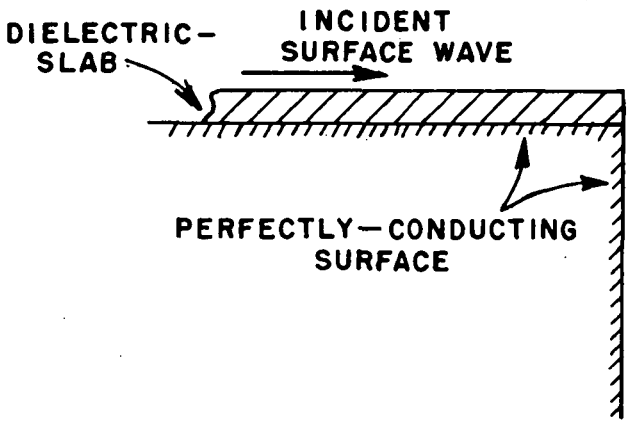

Fig. 3a. The surface wave incident on a dielectric-covered perfectly-conducting right-angled bend.

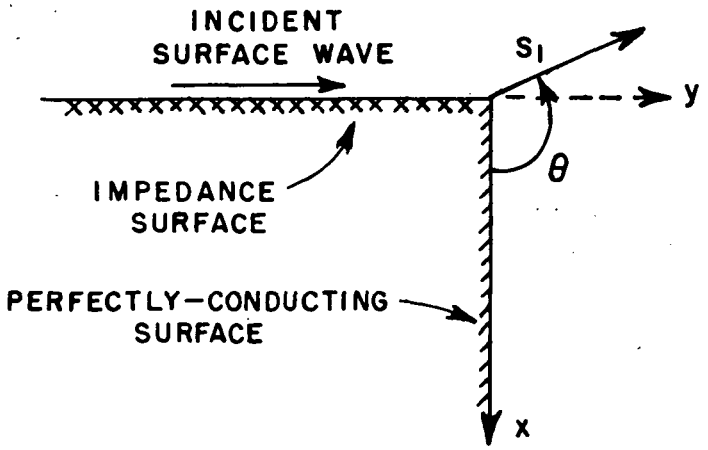

Fig. 3b. Surface impedance model for a dielectric-covered perfectly-conducting right-angled bend.

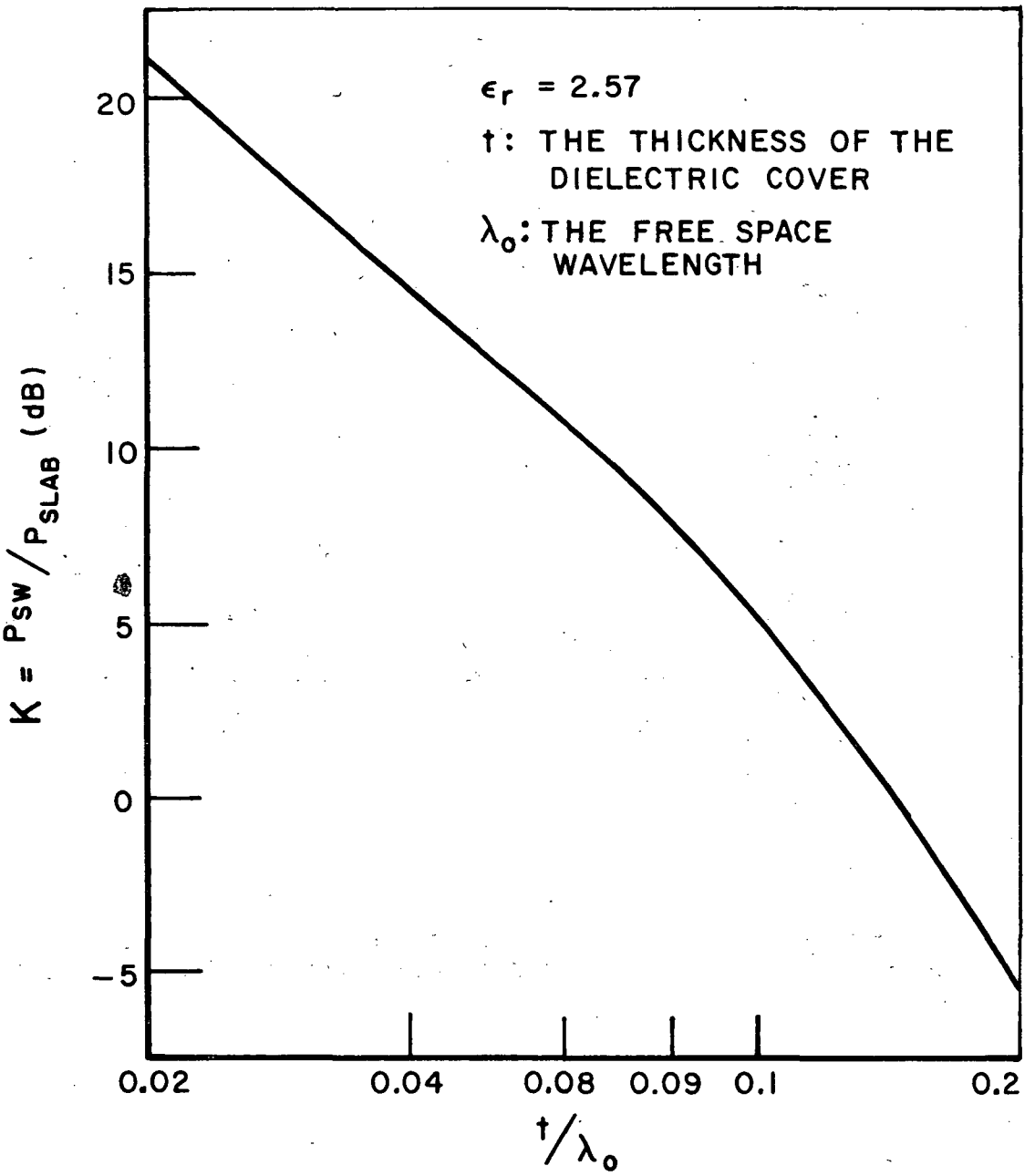

Fig. 4. The power ratio of the field of surface wave to the field inside the slab.

and D_{11} is the diffraction coefficient. From the two preceding equations,

$$(10) \qquad D_{11} = \frac{A \cos \frac{\theta}{3}}{\lambda + jk_o \cos \theta} \sqrt{\frac{2}{\pi k_o}} \, e^{+j\frac{5\pi}{12}} \quad ,$$

where

$$(11) \qquad A = \frac{4j\sqrt{k_o^2 + \lambda^2}}{-3j\sqrt{k_o^2 + \lambda^2}\, I_{1/3} - \sqrt{3}\left(I_{1/3}\, \lambda - I_{2/3}\, k_o\, e^{-j\frac{2\pi}{3}}\right)}$$

$$(12) \qquad I_v = \frac{2\, e^{jv\frac{\pi}{2}} \sin v\theta_s}{k_o \sin v\pi \sin \theta_s}$$

$$(13) \qquad \theta_s = \frac{\pi}{2} + j \sinh^{-1} \frac{\lambda}{k_o} \quad .$$

The field of the reflected surface wave at the impedance boundary is

$$(14) \qquad H_{1s} = H_w R\, e^{-j\beta s_o} \quad ,$$

where β is given by Eq. (4), s_o is the distance along the impedance surface measured from the edge, and the reflection coefficient of the surface wave is

$$(15) \qquad R = -\frac{\cos \frac{1}{3}(\theta_s + \pi)}{\cos \frac{1}{3}(\theta_s - \pi)} \quad .$$

In treating the radiation from thicker dielectric covers, where the field within the cover cannot be ignored, it is apparent that the above approximation is inadequate. In particular, we note that there is a significant contribution from the internal field in the form of radiation from the vertical end faces of the slab at A-A' and B-B' in Fig. 1.

This radiation from the vertical end faces of the dielectric cover is taken into account by using a Kirchhoff-type approximation, where the total electric field within the dielectric cover at its end face radiates in the presence of a right-angle wedge. Here again the dielectric cover is approximated by an impedance surface. The equivalent source of this radiation is the magnetic surface current

$$(16) \qquad K_s = \frac{\beta}{\omega\varepsilon\varepsilon_o r}\,(1+R)\,H_w\,\frac{\cos k_x(x-t)}{\cos k_x t}\quad ,$$

where $k_x = \sqrt{k^2 - \beta^2}$. The magnetic surface current radiates in the presence of the wedge structure shown in Fig. 5. R is calculated from Eq. (15). To obtain an integral representation for the magnetic field, one seeks the Green's function which satisfies the mixed boundary conditions.

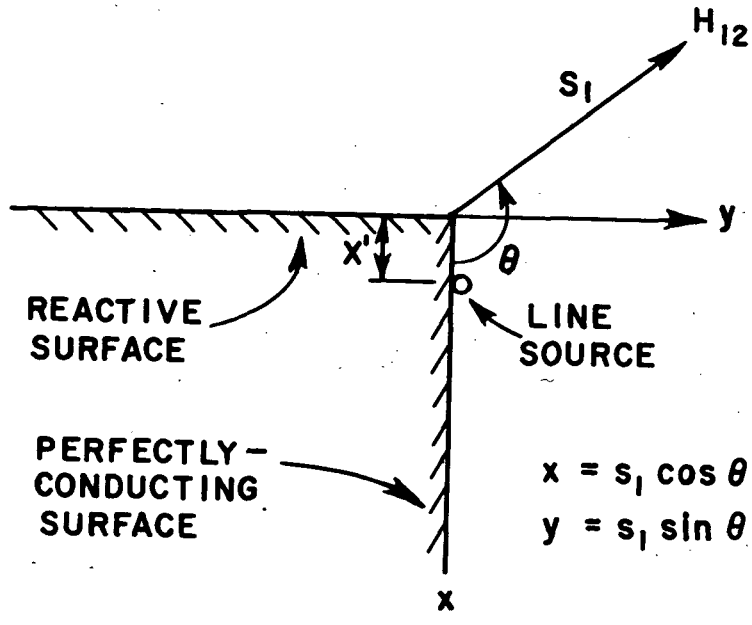

Fig. 5. Line source located at ($x = x'$ $\theta = 0^o$) on a right angled wedge with mixed boundary conditions.

$$\text{(17a)} \qquad \frac{\partial G}{\partial x} - \lambda G = 0 \qquad , \quad x = 0, \quad y < 0$$

and

$$\text{(17b)} \qquad \frac{\partial G}{\partial y} = 0 \qquad , \quad y = 0, \quad x > 0$$

This type of the problem can be solved by the introduction of an auxiliary function which is a linear combination of the field and its cartesian derivatives. The auxiliary function is chosen in such a way that it satisfies the wave equation and simple homogeneous boundaries conditions. Once the auxiliary function is obtained, the original field can be determined by solving a partial differential equation. This idea is due to Stoker [4] and Lewy [5] who studied problems in water wave theory. The far-zone Green's function, $G(s_1,\theta;x',0)$, is derived in Appendix 1, where it is shown that

$$\text{(18)} \qquad G(s_1,\theta;x',0) \sim g(\theta;x',0) \frac{e^{-jk_0 s_1}}{\sqrt{s_1}}$$

in which $g(\theta;x',0)$ is a far-field pattern function which is independent of s_1.

The diffracted field is then

$$\text{(19)} \qquad H_{12} = H_w D_{12} \frac{e^{-jk_0 s_1}}{\sqrt{s_1}}$$

where D_{12} is the diffraction coefficient associated with the diffracted field H_{12}. From Appendix 1,

$$\text{(20)} \qquad D_{12}(\theta) = j\beta(1+R) \int_0^t \frac{\cos k_x(x'-t)}{\cos k_x t} g(\theta;x',0)dx' \quad .$$

This diffracted field contributes a second term to the diffracted field H_{11} previously obtained. Thus the total field diffracted from a wedge with a dielectric cover on one surface can be approximated as

$$\text{(21)} \qquad H_1(s_1,\theta_1) = H_{11}(s_1,\theta_1) + H_{12}(s_1,\theta_1)$$

$$= H_w[D_{11}(\theta_1) + D_{12}(\theta_1)] \frac{e^{-jk_0 s_1}}{\sqrt{s_1}}$$

where it is more appropriate to replace θ by θ_1 here. With the inclusion of the H_{12} term, the surface impedance approximation can be used to treat the radiation from dielectric covers of increased thickness, as will be demonstrated in the next section.

The field diffracted from the termination of the dielectric cover is in turn incident on the edge of the ground plane at a distance h directly below it. This gives rise to

$$(22) \qquad H_2(s_2,\theta_2) = H_w[D_{11}(\tfrac{3\pi}{2}) + D_{12}(\tfrac{3\pi}{2})] \frac{e^{-jk_0 h}}{\sqrt{h}} \tfrac{1}{2} D_h(\theta_2,0) \frac{e^{-jk_0 s_2}}{\sqrt{s_2}} ,$$

a doubly-diffracted contribution from the edges C and D in Fig. 1. Here $D_h(\theta_2,0)$ is the hard scalar diffraction coefficient given in Reference 6. The factor of ½ must be introduced at grazing incidence ($\theta_2' = 0$) on the edge. This contribution from the lower edges of the ground plane has little effect on the pattern in the illuminated region, which is dominated by the field directly radiated from the slot plus the singly-diffracted contributions from the terminations of the dielectric cover. On the other hand, this contribution appears as a significant ripple in the pattern of the shadow region below the dielectric-covered ground plane. Thus, with reference to Fig. 1, the total field for $y > 0$

$$(23) \qquad H = \begin{cases} H_0 + H_{1A} + H_{1B} + H_{2D} & , \quad x > 0 \\ H_{1B} + H_{2C} + H_{2D} & , \quad x < 0 \end{cases}$$

in which the first subscript 0,1,2 denotes whether the field is incident, singly-diffracted or doubly-diffracted and the second subscript indicates the edge from which the diffracted ray originates. The expression for H when $y < 0$ is similar.

A computer program based on Eq. (23) has been developed; it is described in Appendix 3. In using this program it should be noted that ε_r cannot be very close to 1, nor can the thickness of the cover t be very close to zero. Thus, the present solution does not reduce to the slot in the ground plane without a dielectric cover. The reason for this limitation is that the distance from the slot required to establish the dominance of the surface wave field increases as $\varepsilon_r \to 1$, $t \to 0$. Under these circumstances the field at the termination of the cover is not simply that of the surface wave;however, this field can

be determined so that the transition to the case of the ground plane without a cover can be made. But this must await further work. The pattern calculation shown in Fig. 7 is based on a separate solution where the surface wave emanating from the slot is replaced by a space wave propagating along the surface of the ground plane, and the diffraction coefficients for the hard boundary are employed at edges A and B.

III. NUMERICAL RESULTS

Eq. (23) is used to calculate the far zone patterns of the configuration shown in Fig. 1. In each case the ground plane length L is 12.13 inches, the height h is 1.71 inches and its width (in the direction perpendicular to the page) is 22 inches. A 0.5 inch by 0.062 inch slot is positioned 0.1 inch to the right of the center of the ground plane, thereby introducing a slight asymmetry in the patterns. The axis of the slot is parallel to the edges shown in Fig. 1. The precise dimensions are shown in Fig. 6. The slot is excited at frequencies so that only the TM_0 surface wave mode can exist. The patterns are calculated in the plane of symmetry normal to the axis of the slot for various frequencies and cover thickness.

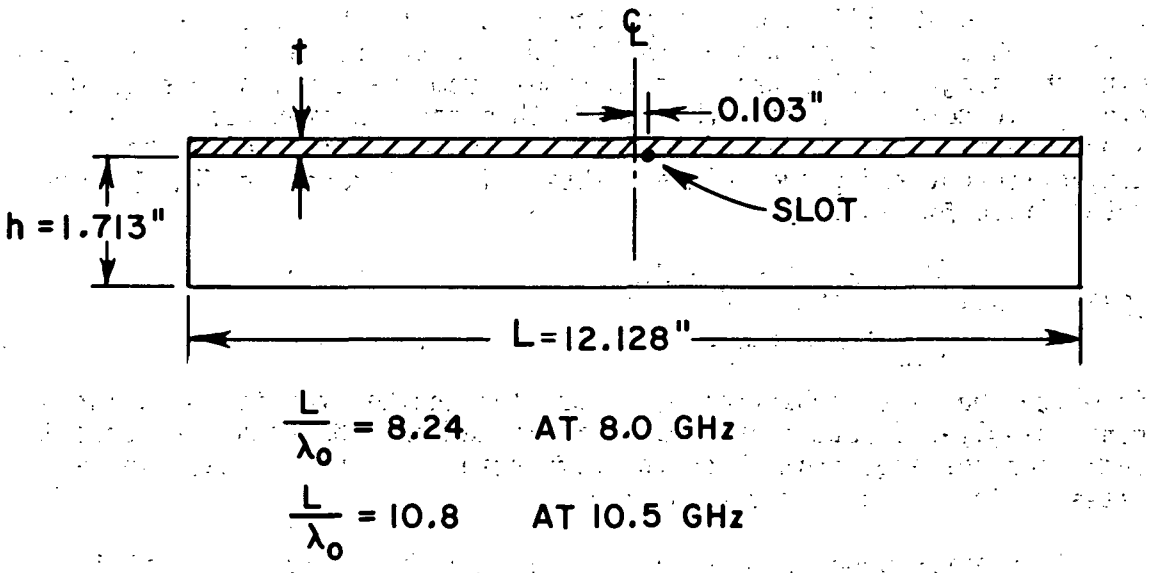

Fig. 6. Experimental dielectric-covered ground plane with slot.

The calculated and measured patterns for a slot in the ground plane without a dielectric cover are shown in Fig. 7. As explained at the end of section II, a separate calculation via the geometrical

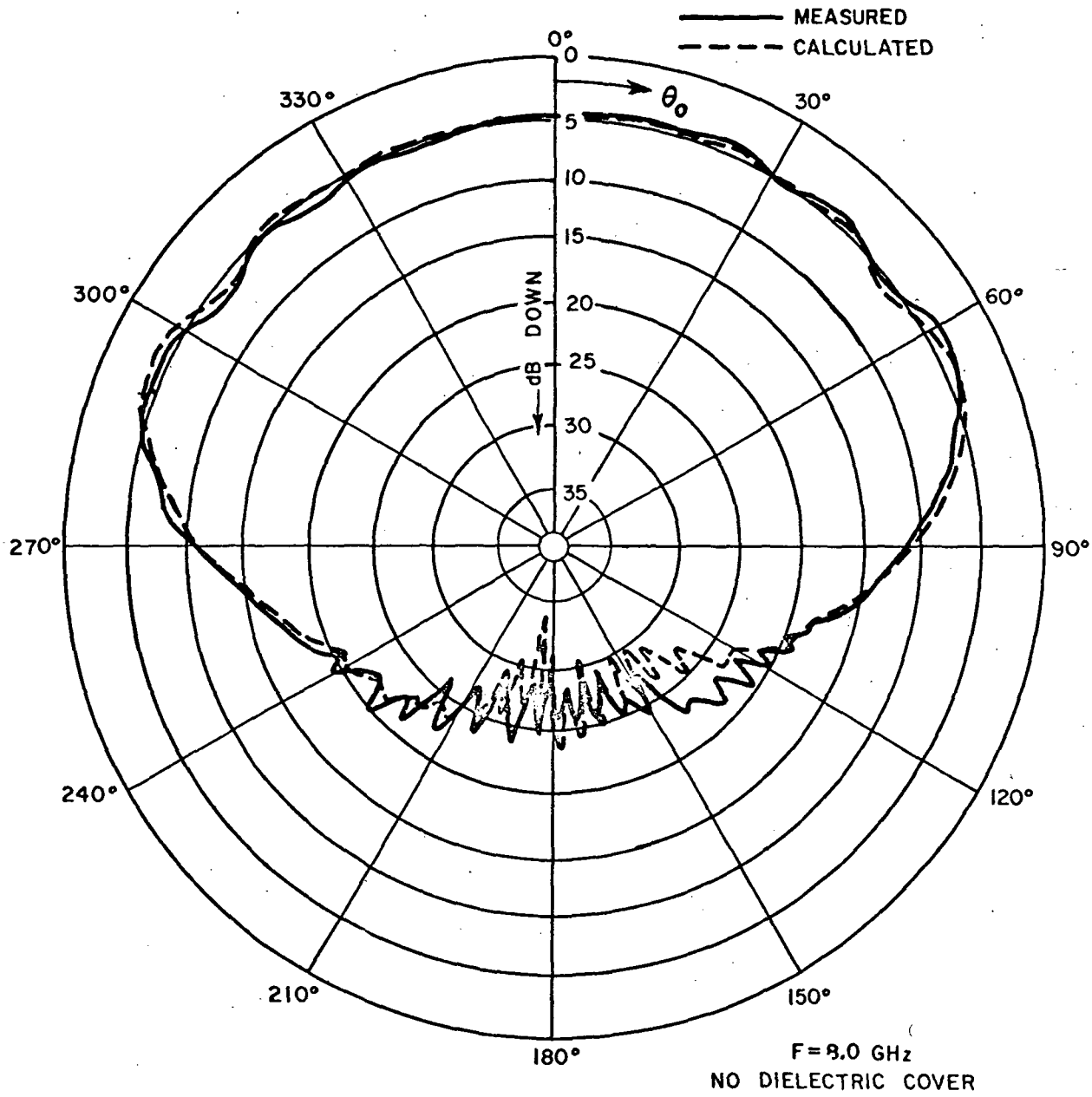

Fig. 7. Pattern of a slot in a perfectly-conducting ground plane. Frequency = 8 GHz.

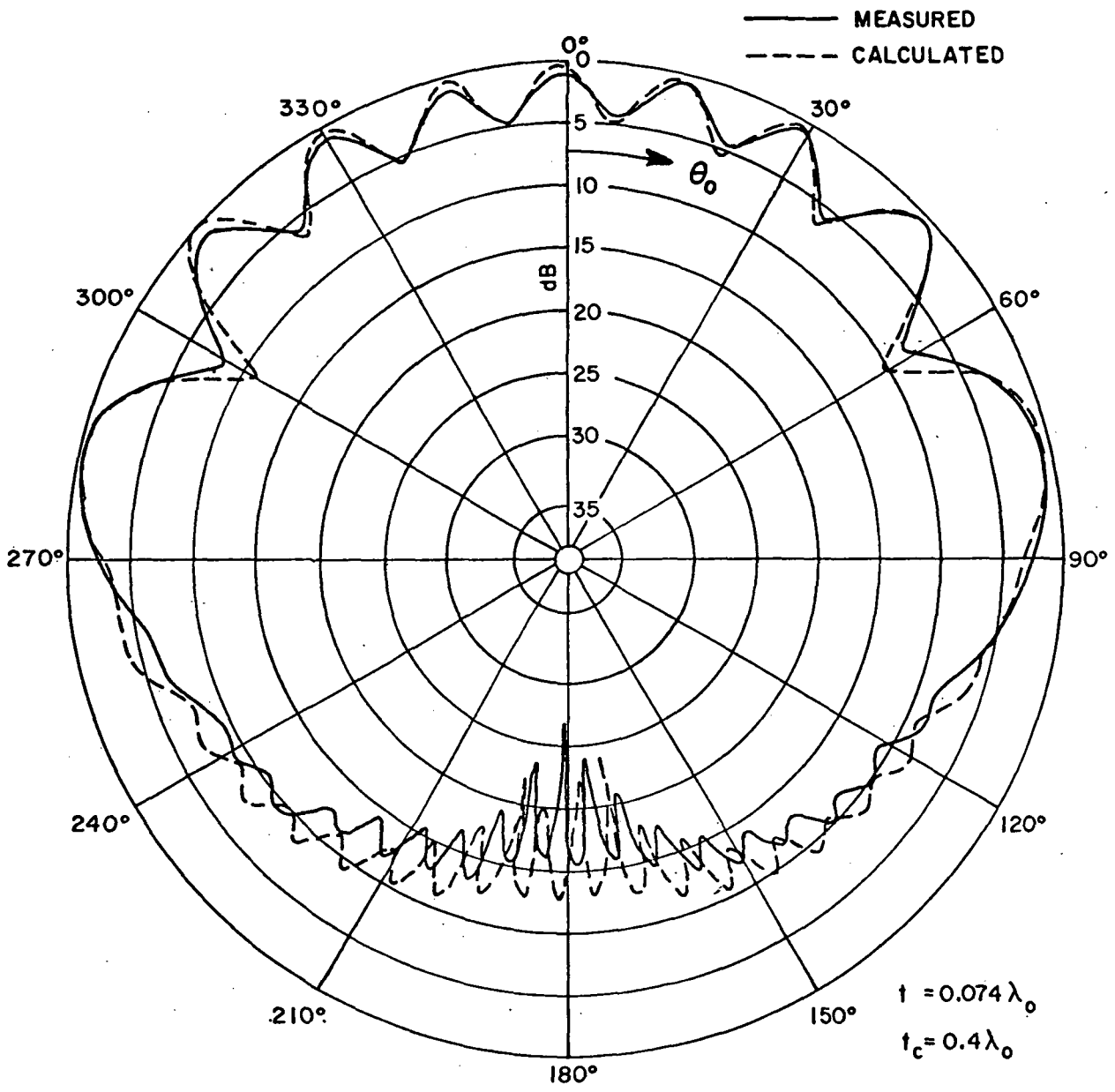

Fig. 8. Pattern of a slot in a dielectric-covered ground plane. Frequency = 8 GHz, t = 0.11 inch, ε_r = 2.57.

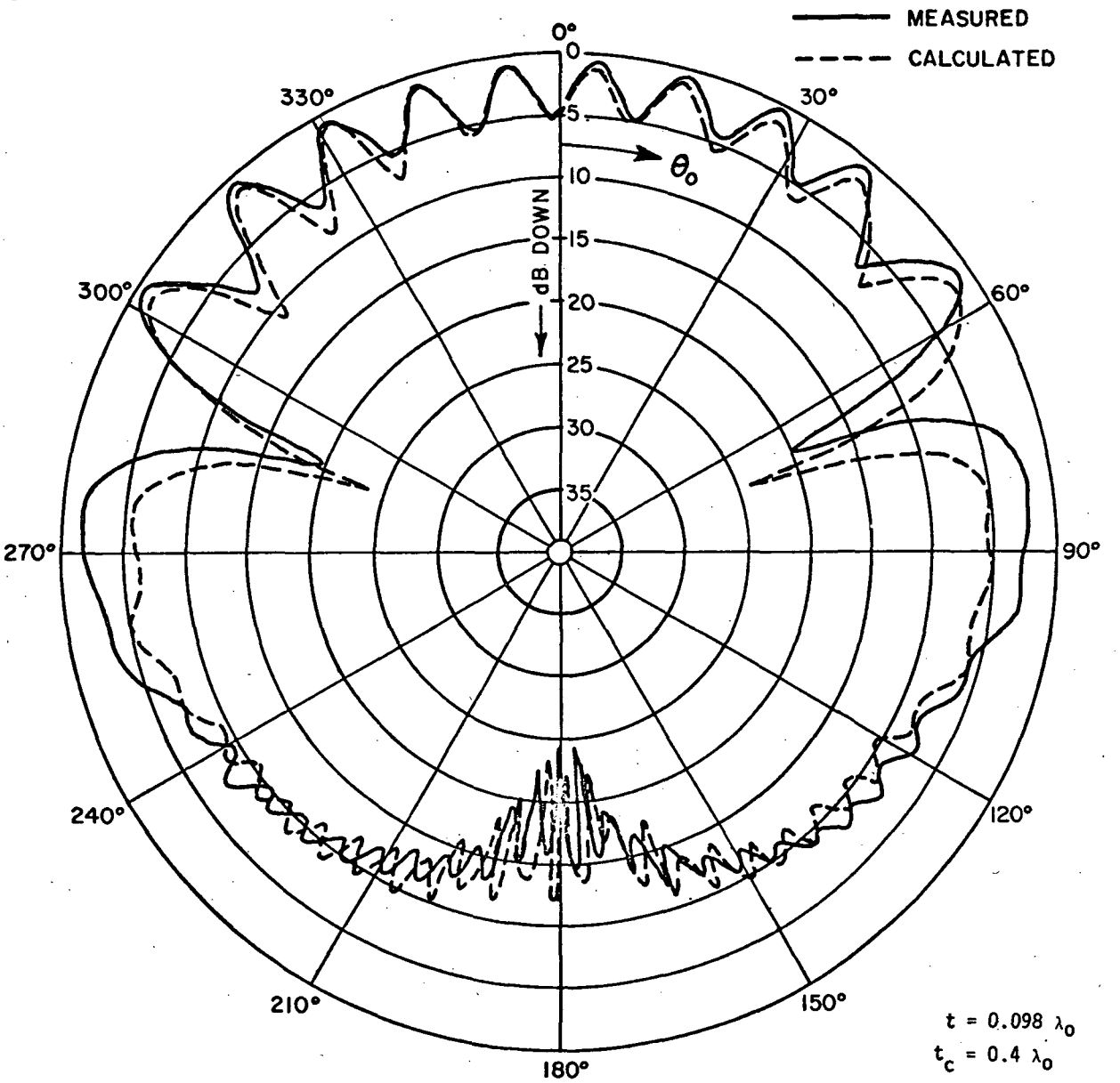

Fig. 9. Pattern of a slot in a dielectric-covered ground plane. Frequency = 10.5 GHz. t = 0.11 inch, ε_r = 2.56.

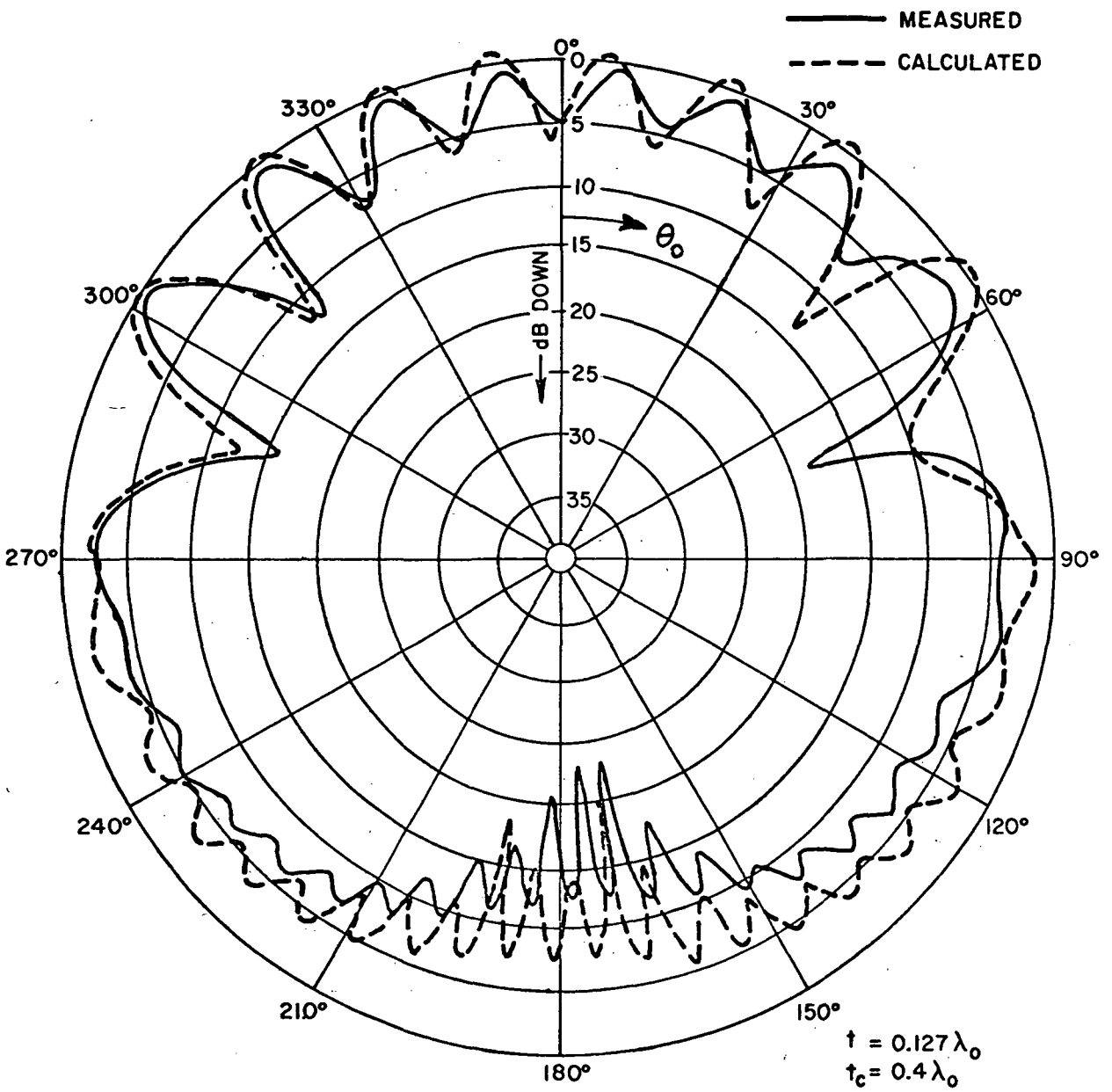

Fig. 10. Pattern of a slot in a dielectric-covered ground plane. Frequency = 8 GHz. t = 0.1875 inch, $\varepsilon_r = 2.56$.

theory of diffraction is required in this case. Typical calculated and measured* patterns for the dielectric-covered slot are shown in Figs. 8, 9 and 10; in these figures t_c is the thickest dielectric cover in which only the dominant TM_0 surface wave mode can propagate. In the illuminated region, the position and level of the lobes of the two patterns are seen to compare in detail, and overall the comparison of the two patterns is good. In Fig. 8, where the dielectric cover is relatively thin, the end face radiation contribution $H_{12}(\theta_1)$ of Eq. (21) is unimportant and could be neglected. However, for the thicker dielectric covers of Figs. 9 and 10, this contribution is significant. The importance of H_{12} is illustrated in Fig. 11, where

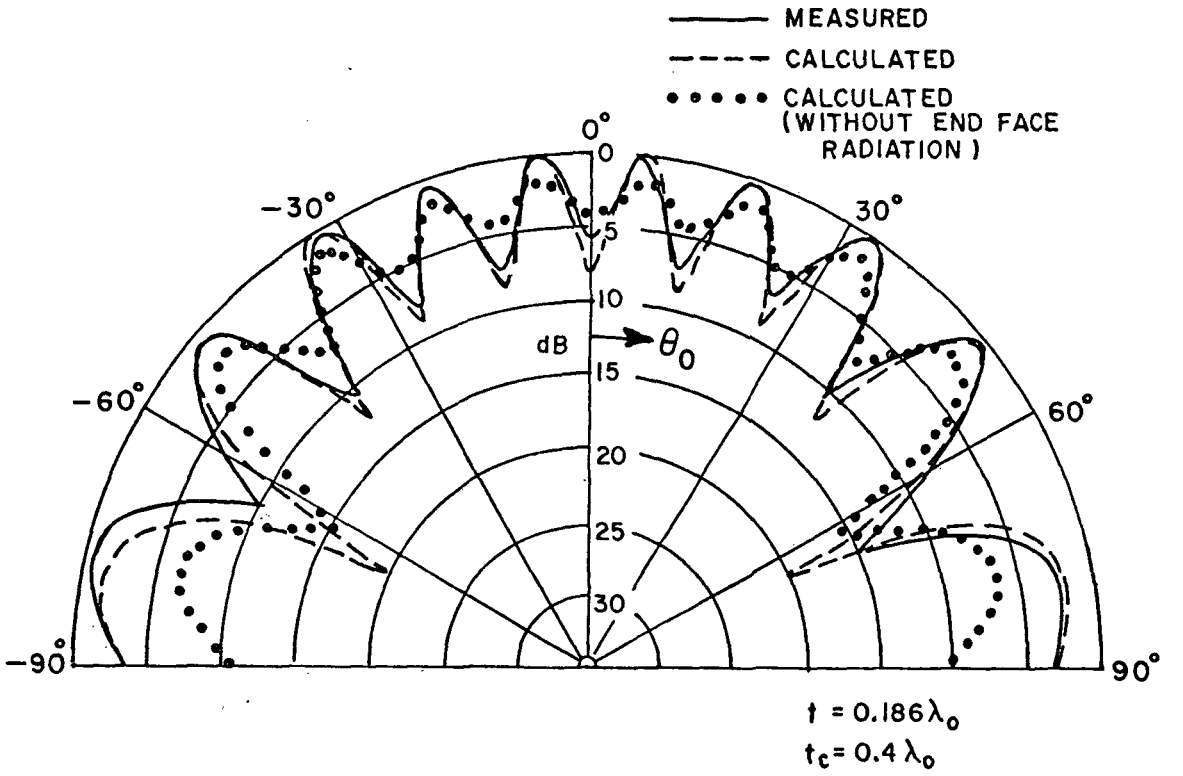

Fig. 11

*The measured patterns were provided by Mr. W. F. Croswell of the NASA Langley Research Center, Hampton, Va.

patterns calculated with and without this contribution are shown in the illuminated region. It is seen that this contribution is required to bring the calculated pattern into agreement with the measured pattern. In this case the slot is positioned in the center of the ground plane, so the symmetry of the measured pattern with respect to 90° is an indication of its accuracy.

The patterns are very sensitive functions of the parameters, such as the thickness of the dielectric cover and the frequency. This is shown in Fig. 12, where it is seen that a frequency change of less than two percent causes a substantial change in pattern detail. This sensitivity to slight changes in the parameters could in part account for the differences noted between the calculated and measured patterns.

The presence of a dielectric cover on the ground plane substantially increases the pattern level in the shadow region when the dielectric is lossless. As the loss tangent, tan δ, of the dielectric increases, so does the attenuation of the surface wave incident on the termination of the dielectric cover. This in turn weakens the contributions of the singly- and doubly-diffracted fields. As a result, the ripples in the patterns in the illuminated region diminish, and the level of radiation in the shadow region is reduced, as shown in the calculated patterns of Figs. 13 and 14. In Fig. 14, when tan δ = 0.2, the diffracted field components have been so reduced, the pattern is essentially that of the directly-incident (geometrical optics) field.

IV. CONCLUSIONS

The calculated and measured patterns compare well, which justifies the use of the geometrical theory of diffraction in this type of problem together with the approximations which have been used to find the diffraction coefficient. In particular, the method employed to extend the approximation of the impedance boundary in treating edge diffraction appears to be useful. The patterns of the slot in the dielectric covered ground plane are very sensitive functions of the parameters, such as the thickness of the dielectric cover and the frequency. The presence of the cover substantially increases the pattern level in the shadow region when the dielectric is lossless. As the loss tangent increases, the ripples in the patterns in the illuminated region diminish and the level of radiation in the shadow region is reduced.

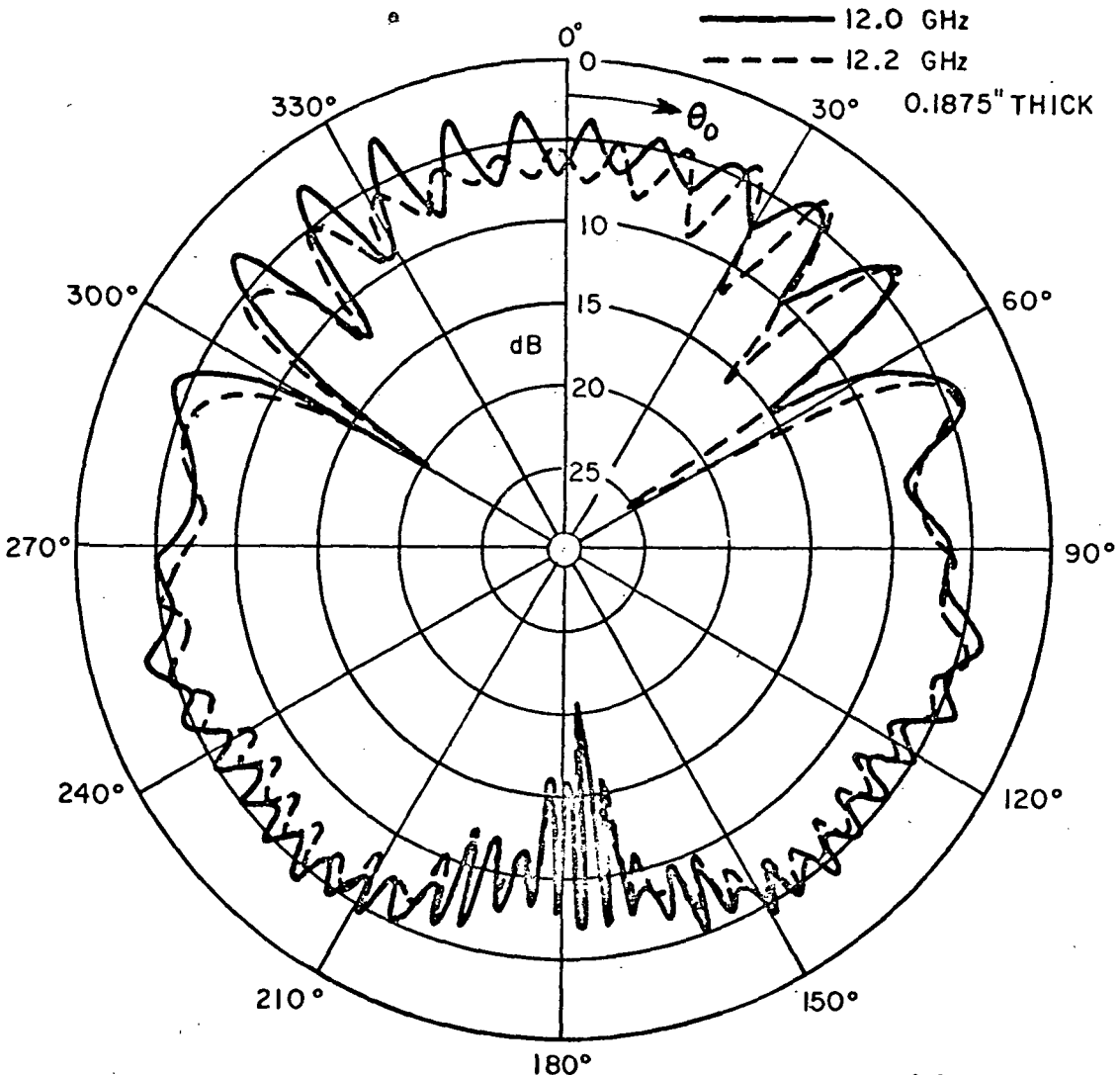

Fig. 12. Patterns of a slot in a dielectric-covered ground plane: calculated patterns at slightly different frequencies.

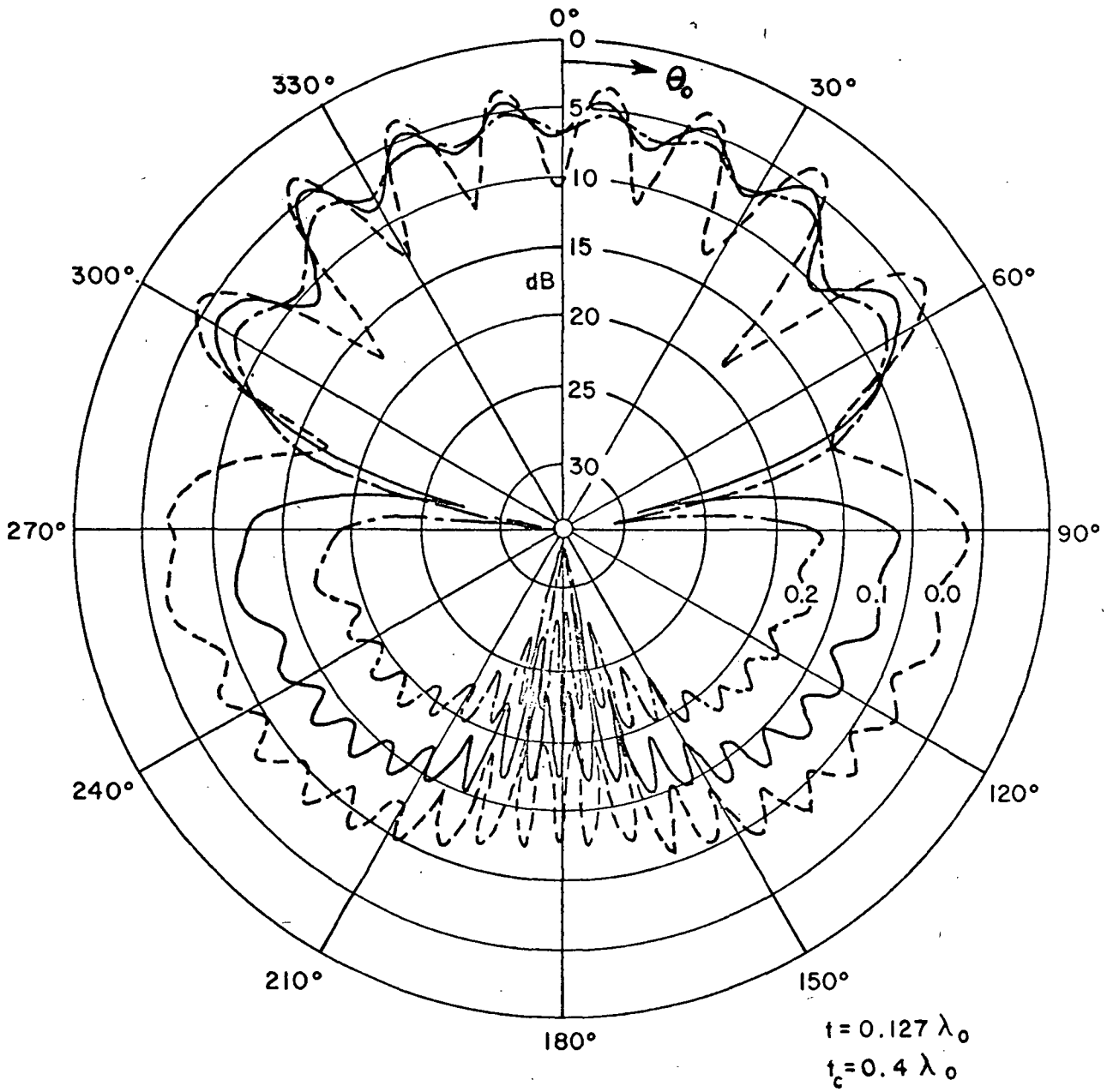

Fig. 13. Patterns of a slot in a dielectric-covered ground plane. Frequency = 8 GHz, t = 0.1875 inch, $\varepsilon_r = 2.56\ (1\text{-}j\ \tan\delta)$. The values of $\tan\delta$ are shown on the patterns.

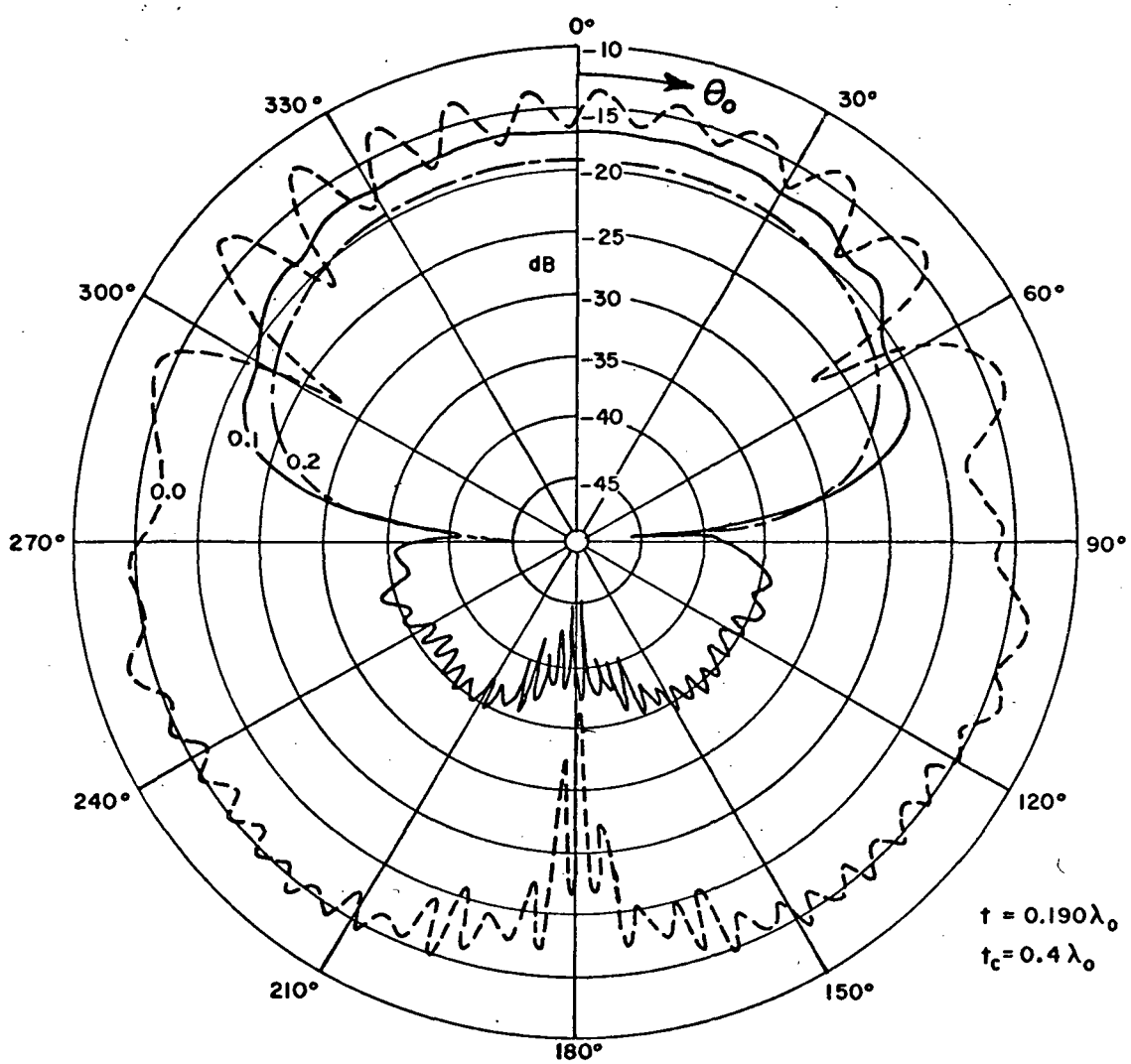

Fig. 14. Patterns of a slot in a dielectric-covered ground plane. Frequency = 12 GHz, t = 0.1875 inch, $\varepsilon_r = 2.57\ (1\text{-}j\ \tan\delta)$. The values of $\tan\delta$ are shown on the patterns.

REFERENCES

[1] M. C. Bailey and W. F. Croswell, "Pattern Measurements of Slot Radiators in Dielectric-Coated Metal Plates," IEEE Trans. on Antennas and Propagation, Vol. AP-15, No. 6, pp. 824-825, November 1967.

[2] J. B. Keller, "Geometrical Theory of Diffraction," J. Opt. Soc. Am., 52, pp. 116-130, 1962.

[3] T. S. Chu, R. G. Kouyoumjian, F. C. Karal and S. N. Karp, "The Diffraction of Surface Waves by a Terminated Structure in the Form of a Right-Angle Band," IRE Trans. on Antennas and Propagation, Vol. AP-10, No. 6, pp. 679-686, November 1962.

[4] J. J. Stoker, "Surface Waves in Water of Variable Depth," Quarterly of Appl. Math., 5, 1 (1947).

[5] H. Lewy, "Waves on Sloping Beaches," Bull. AMS, 52, 737 (1946).

[6] P. H. Pathak and R. G. Kouyoumjian, "The Dyadic Diffraction Coefficient for a Perfectly Conducting Wedge," Report 2183-4, 5 June 1970, The Ohio State University ElectroScience Laboratory, Department of Electrical Engineering; prepared under Contract AF 19(625)-5929 for Air Force Cambridge Research Laboratories. (AFCRL 69 0546) (AD 707 827)

[7] Samuel N. Karp, "Two Dimensional Green's Function for a Right Angled Wedge Under an Impedance Boundary Condition," Communications on Pure and Applied Math., Vol. XIII, pp. 203-216, 1960.

[8] S. N. Karp and F. C. Karal, "Vertex Excited Surface Waves on One Face of a Right Angled Wedge," N.Y.U., Inst. Math. Sci., Div. E M Res., Research Report No. AM-124, January 1959.

APPENDIX I
THE GREEN'S FUNCTION FOR A RIGHT-ANGLED WEDGE WITH AN IMPEDANCE BOUNDARY CONDITION

Consider a right-angle wedge $y = 0$, $x > 0$ and $x = 0$, $y < 0$, and suppose there is a line source located at $(\rho',0)$ as shown in Fig. 5.

The Green's function G satisfies the following differential equation:

$$(\nabla^2 + k_0^2)\, G(x,y;x',y') = -\delta(x-x')\,\delta(y-y') \tag{A-1}$$

where

$$\begin{cases} x = \rho \cos\theta \\ y = \rho \sin\theta \end{cases}$$

and

$$\begin{cases} x' = \rho' \cos\theta' = \rho' \\ y' = \rho' \sin\theta' = 0 \end{cases} .$$

The boundary conditions of interest here are given by

$$\frac{\partial G}{\partial y} = 0 \quad , \quad y = 0, \quad x > 0 \tag{A-2a}$$

$$\frac{\partial G}{\partial x} - \lambda G = 0 \quad , \quad x = 0, \quad y < 0 \quad . \tag{A-2b}$$

Also,

(A-2c) G satisfies the Sommerfeld radiation condition,

and

(A-2d) G is finite except at (x',y').

λ is equal to $-j\, k_0\, Z_s/Z_0$, where Z_s is the surface impedance given by Eq. (1), and in problem of interest here, Z_s is such that $\mathrm{Re}\,\lambda > 0$. Our treatment of this problem closely parallels that of Karp [7], except for the manner in which the unknown constant A, which will be encountered later, is found.

Let us make a transformation

$$(A\text{-}3) \qquad \bar{V}(x,y) = \left(\frac{\partial}{\partial x} - \lambda\right) G(x,y) \quad ;$$

then $\bar{V}$ must satisfy the following differential equation:

$$(A\text{-}4) \qquad (\nabla^2 + k_0^2)\, \bar{V}(x,y) = \left(-\frac{\partial}{\partial x} + \lambda\right) \delta(x-x')\, \delta(y-y') \quad .$$

Using the relationship $(\partial/\partial x)\delta(x-x') = -(\partial/\partial x')\delta(x-x')$,

$$(A\text{-}5) \qquad (\nabla^2 + k_0^2)\, \bar{V}(x,y) = \left(\frac{\partial}{\partial x'} + \lambda\right) \delta(x-x')\, \delta(y-y') \quad .$$

The boundary conditions for $\bar{V}(x,y)$ are then

$$(A\text{-}6a) \qquad \frac{\partial \bar{V}}{\partial y} = 0 \qquad , \quad y = 0, \quad x > 0$$

$$(A\text{-}6b) \qquad \bar{V} = 0 \qquad , \quad x = 0, \quad y < 0 \quad .$$

The function $\bar{V}(x,y)$ need not be finite at the origin since it involves a differentiation of G. The solution to Eq. (A-5) can be obtained by first solving for the Green's function $G_0(x,y;x',y')$, which satisfies the differential equation

$$(A\text{-}7) \qquad (\nabla^2 + k_0^2)\, G_0(x,y;x',y') = -\delta(x-x')\, \delta(y-y')$$

together with the same boundary conditions

$$(A\text{-}8a) \qquad \frac{\partial G_0}{\partial y} = 0 \qquad , \quad y = 0, \quad x > 0$$

$$(A\text{-}8b) \qquad G_0 = 0 \qquad , \quad x = 0, \quad y < 0$$

and the radiation condition.

It can be shown that

$$(A\text{-}9)\qquad G_0(x,y;x',y') = -\frac{2j}{3}\sum_{n=0}^{\infty}\cos\frac{2n+1}{3}\theta\cos\frac{2n+1}{3}\theta' J_{\frac{2n+1}{3}}(k\rho_<) \cdot H^{(2)}_{\frac{2n+1}{3}}(k\rho_>),$$

where J_ν is Bessel function of order ν and $H^{(2)}_\nu$ is a Hankel function of second kind of order ν.

By applying the operator $-(\partial/\partial x' + \lambda)$ to $G_0(x,y;x',y')$, we can obtain the following solution for $\overline{V}(x,y)$:

$$(A\text{-}10)\qquad \overline{V}(x,y;x',y') = -\left(\frac{\partial}{\partial x'} + \lambda\right) G_0(x,y;x',y') \quad .$$

The complete solution for $\overline{V}(x,y)$ is

$$(A\text{-}11)\qquad \overline{V}(x,y;x',y') = -\left(\frac{\partial}{\partial x'} + \lambda\right) G_0(x,y;x',y') + \sum_{n=0}^{\infty} a_n \cos\frac{2n+1}{3}\theta\, H^{(2)}_{\frac{2n+1}{3}}(k\rho).$$

The last summation contains the class of admissible singular solutions which satisfy the homogeneous equation for $\overline{V}$. Since $\overline{V}$ cannot be too singular at the edge, the only admissible function of the singular class is the first term; hence,

$$(A\text{-}12)\qquad \begin{aligned} a_0 &= c_1 \quad , \\ a_n &= 0 \quad , \quad n \geq 1 \quad . \end{aligned}$$

A particular solution of (A-3) is

$$(A\text{-}13)\qquad G_p(x,y) = -e^{\lambda x}\int_x^{\infty} e^{-\lambda \xi}\,\overline{V}(\xi,y)\,d\xi \quad .$$

The existence of the integral is guaranteed since $\mathrm{Re}\ \lambda \geq 0$.

The function $G_p(x,y)$ does not satisfy all the conditions of the problem, for it is not a wave function on the negative x-axis, since its y derivative is not continuous there. This defect can be remedied by adding a complementary solution for G, obtained from (A-3), to (A-13); thus we obtain

$$(A\text{-}14)\quad G(x,y;x',y') = G_p + \begin{cases} c_2 e^{\lambda x + j\sqrt{k_0^2+\lambda^2}\, y} & , \quad y < 0 \\ 0 & , \quad y > 0 \end{cases}$$

c_1 and c_2 are then determined by imposing the boundary conditions

$$(A\text{-}15a)\quad G(x,0^+) - G(x,0^-) = 0 \ , \quad x < 0$$

and

$$(A\text{-}15b)\quad \frac{\partial G(x,0^+)}{\partial y} - \frac{\partial G(x,0^-)}{\partial y} = 0 \ , \quad x < 0 \ .$$

Numerically it is very difficult to obtain c_1 and c_2. This difficulty can be avoided if we choose a suitable function [7], H(x,y), which has the same singular property as $H_{1\beta}^{(2)}(k_0\rho)$ and is a homogeneous solution for $\overline{V}$.

Let us consider the Green's function N which satisfies

$$(A\text{-}16)\quad (\nabla^2 + k_0^2)\, N(x,y;x',y') = -\,\delta(x-x')\,\delta(y-y')$$

with the boundary conditions

$$(A\text{-}17a)\quad \frac{\partial N}{\partial y} = 0 \qquad y = 0, \quad x > 0$$

$$(A\text{-}17b)\quad \frac{\partial N}{\partial x} = 0 \qquad x = 0, \quad y < 0$$

together with the

(A-17c) Radiation Condition.

It can be shown that

$$(A\text{-}18)\quad N(x,y;x',y') = -\frac{j}{3}\sum_{n=0}^{\infty}\varepsilon_n \cos\frac{2n}{3}\theta \cos\frac{2n}{3}\theta' \, J_{\frac{2n}{3}}(k\rho_<)\, H^{(2)}_{\frac{2n}{3}}(k\rho_>)$$

where ε_n is the Neumann's constant

$$\varepsilon_n = \begin{cases} 1 & n = 0 \\ 2 & n = 1,2,\cdots . \end{cases}$$

$$(A\text{-}19)\quad \text{Let } H = \frac{\partial G}{\partial x'} + \frac{\partial N}{\partial x}$$

$$(A\text{-}20)\quad \therefore (\nabla^2 + k_0^2)\, H = 0 \quad .$$

$H(x,y)$ is thus a solution of the homogeneous wave equation with the boundary conditions

$$(A\text{-}21a)\quad \frac{\partial H}{\partial y} = 0 \qquad y = 0, \quad x > 0$$

$$(A\text{-}21b)\quad H = 0 \qquad x = 0, \quad y < 0$$

together with

(A-21c) the Radiation Condition.

Note that the leading term of $\partial N/\partial x$ has the same singular property as $H^{(2)}_{\frac{1}{3}}(k_0\rho)$.

The complete solution for $\overline{V}$ is then

$$(A\text{-}22)\quad \overline{V}(x,y;x',y') = -(\frac{\partial}{\partial x'} + \lambda)\, G_0(x,y;x',y') + A\, H(x,y;x',y')$$

where A is a constant to be determined.

That G satisfies the wave equation can be shown from the fact that

$$G_x = \overline{V} + \lambda\, G$$

$$G_{xx} = \overline{V} + \lambda\, \overline{V} + \lambda^2\, G$$

also $$\overline{V}_{yy} = -\overline{V}_{\S\S} - k_o^2\, \overline{V} + \left(\frac{\partial}{\partial x'} + \lambda\right) \delta(\S - x')\, \delta(y - y')$$

$$\therefore\ G_{xx} + G_{yy} + k_o^2\, G =$$

$$\overline{V}_x + \lambda\, \overline{V} + \lambda^2\, G - e^{\lambda x} \int_x^\infty e^{-\lambda \S}\, \overline{V}_{yy}(\S, y)\, d\S + k_o^2\, G \quad .$$

Integrating by parts twice in the above integral,

$$G_{xx} + G_{yy} + k_o^2\, G = -\left(\frac{\partial}{\partial x'} + \lambda\right) e^{\lambda(x-x')}\, \delta(y-y') \int_x^\infty \delta(\S - x')\, d\S$$

$$= -\left(\frac{\partial}{\partial x'} + \lambda\right) e^{\lambda(x-x')}\, u(x-x')\, \delta(y-y')$$

$$= -e^{\lambda(x-x')}\, \frac{\partial}{\partial x}\, u(x-x')\, \delta(y-y')$$

$$= \delta(x-x')\, \delta(y-y')$$

where $u(x-x')$ is a unit step function.

In the far zone, we observe that G_o, N, G and $\overline{V}$ have the asymptotic form

(A-23a) $$G_o \simeq \frac{e^{-jk_o\rho}}{\sqrt{\rho}} g_o(\theta; x', y')$$

(A-23b) $$N \simeq \frac{e^{-jk_o\rho}}{\sqrt{\rho}} n(\theta; x', y')$$

(A-23c) $$G \simeq \frac{e^{-jk_o\rho}}{\sqrt{\rho}} g(\theta; x', y')$$

and

(A-23d) $$\bar{V} \simeq \frac{e^{-jk_0\rho}}{\sqrt{\rho}} u(\theta;x',y') \quad .$$

Since the far-zone field is of interest, only those terms which are of $O(1/\sqrt{\rho})$ are retained, the operator $\partial/\partial x$ can be approximated by $-j\,k\cos\theta$; thus we obtain

(A-24) $$G(x,y;x',y') \simeq \frac{\left[(A-1)\frac{\partial}{\partial x'} - \lambda\right] G_0 + j\,k_0 \cos\theta\, A\, N}{j\,k_0 \cos\theta - \lambda} \quad .$$

Hwang [*] determines the constant A by transforming the function G_0 and N into the integral representations which are then evaluated asymptotically by the modified Pauli-Clemmow method of steepest descent. From the asymptotic solution, we can identify the ray-optical behavior of the field. The pole contributions give rise to the geometrical optics field which is the sum of the incident field and the reflected field. From this we obtain

(A-25) $$A = 1 \quad .$$

Thus,

(A-26) $$G(x,y;x',y') \simeq \frac{j\,k_0 \cos\theta\, N - \lambda\, G_0}{j\,k_0 \cos\theta - \lambda}$$

in the far zone, where N and G_0 are given by Eqs. (23a) and (23b).

*Hwang, Y.M., "Electromagnetic and Scalar Diffraction by a Right-angled Wedge with a Uniform Surface Impedance", to appear.

APPENDIX II
ON CALCULATING THE COMPLEX ROOT OF A TRANSCENDENTAL EQUATION

The problem of finding the complex roots of a transcendental equation is usually reduced to the problem of finding the roots of two simultaneous nonlinear equations. The two nonlinear equations occur because the real and imaginary part of a complex function must also equal zero when the complex function $f(Z) = 0$. The method of finding the roots of simultaneous, nonlinear equations has been discussed in many books; but sometimes it is tedious to reduce a complex function to two real nonlinear functions. In this appendix we point out that Newton's method for the real roots of a real function can be extended to find the complex roots of a complex function.

Suppose that we seek a solution Z_o of a function $f(Z,\varepsilon)$ such that

$$f(Z_o,\varepsilon) = 0 \quad , \tag{A-27}$$

where ε is a complex parameter.

Using Taylor's expansion,

$$f(Z_o,\varepsilon) \simeq f(Z_{o1},\varepsilon) + f'(Z_{o1},\varepsilon)\ \Delta Z_{1a} \tag{A-28}$$

where Z_{o1} is an initial estimate of the root, which is assumed to be close to Z_o. For example, Z_{o1} could be found by solving a related problem exactly.

Let

$$\Delta Z_1 = Z_o - Z_{o1} \quad . \tag{A-29}$$

From Eqs. (A-27) and (A-28),

$$\Delta Z_{1a} = -\frac{f(Z_{o1},\varepsilon)}{f'(Z_{o1},\varepsilon)} \simeq \Delta Z_1 \quad . \tag{A-30}$$

Next, replace Z_{o1} by $Z_{o2} = Z_{o1} + \Delta Z_{1a}$, and repeat the procedure; in this way we can generate successive approximation, and after N iterations,

$$(A\text{-}31) \quad Z_o \simeq Z_{o1} + \sum_{i=1}^{N} \Delta Z_{ia} \quad ,$$

where

$$(A\text{-}32) \quad \Delta Z_{ia} = - \frac{f(Z_{oi},\varepsilon)}{f'(Z_{oi},\varepsilon)} \quad .$$

When Z_{o1} is chosen sufficiently close to the root Z_o and $f'(Z_{oj},\varepsilon) \neq 0$, the process will converge, i.e., $|\Delta Z_{i+1,a}| < |\Delta Z_{ia}|$. The iterative procedure can then be terminated when $|\Delta Z_{ia}| < \delta$, where δ is a specified small number.

APPENDIX III
THE FORTRAN IV PROGRAM FOR CALCULATING THE FAR-ZONE RADIATION PATTERN.

```
C PATTERN CALCULATION OF SLOT RADIATOR IN A DIELECTRIC-COATED METAL PLATE
C     THIS PROGRAM IS GOOD ONLY FOR 0 < D < 0.4*LAMDA0
C     LAMDA0 = FREE SPACE WAVE LENGTHS
C     THIS PROGRAM CANNOT BE USED WHEN ESR=1.0 AND/OR D=0.0
C
C     ESR  - RELATIVE DIELECTRIC CONSTANT
C     ESO  - FREE SPACE DIELECTRIC CONSTANT
C     EL   - DIELECTRIC CONSTANT OF LOSSY SLAB
C     D    - THICKNESS OF DIELECTRIC COATING IN INCHES
C     F    - FREQUENCY IN CPS
C     B    - FREE-SPACE WAVE NUMBER
C     BK   - DIELECTRIC WAVE NUMBER FOR LOSSLESS SLAB
C     V1   - THICKNESS OF TRUNCATED GROUND PLANE IN INCHES(NOT INCLUDING
C            THE THICKNESS OF SLAB)
C     W1   - WIDTH OF DIELECTRIC COATING FORM THE SOURCE TO THE RIGHT
C            CORNER IN INCHES
C     XL   - TOTAL WIDHT OF DIELECTRIC COATING IN INCHES
C     XLT  - LOSS TANGENT OF LOSSY SLAB
C     T    - CONVERSION FACTOR(1 INCH = 0.0254METERS)
C     CU   - SURFACE-WAVE ATTENUATION CONSTANT
C     CBETA- SURFACE-WAVE PROPAGATION CONSTANT
C     HGO  - DIRECT RADIATION FIELD
C     HD1  - DIFFRACTION FIELD(RIGHT SIDE)
C     HD2  - DIFFRACTION FIELD(LEFT SIDE)
C     HY   - SLAB RADIATION FIELD
C     HT   - TOTAL RADIATION FIELD
C     FN   - NORMALIZED CONSTANT OF THE TOTAL RADIATION FIELD IN DB AT
C            90-DEGREES
C     HTT  - TOTAL RADIATION FIELD INCLUDING SLAB RADIATION
C     DBHTT-TOTAL RADIATION FIELD IN DB(WITH SLAB RADIATION)
C     PHD  - ASPECT ANGLE IN DEGREES
C
      COMMON BJ(150),BY(150)
      DIMENSION AUH(180),AUHS(180)
      COMPLEX HGO,THETS,B1,B2,B3,A1,A2,A,HD,HT,CCSW,HR,HL,HD1,HD2,HY
      COMPLEX HDT
      COMPLEX CN,CD,C2,HTT
      COMPLEX HYF,HYB,GF,GB
      COMPLEX CCSW1,CCSW2
      COMPLEX HD10,HD20,HR1,HR11,HL1,HL11
      COMPLEX HP,HQ
      COMPLEX DH1,DH2,DH3,DH4,DH5,H
      COMPLEX HD10,HD11,HD20,HD21,DD,DVDR,DVDL
      COMPLEX CSW,CI1,CI2,X
      COMPLEX EL,Z,ZK,CU,CBETA,CESIL,CESR,TS,C1
      PI=3.141592
 1212 READ(5,1111,END=1112)ESR,F,FN,D,XL,W1,V1,XLT
 1111 FORMAT(F4.2,E10.3,F6.2,4F7.4,E9.2)
      W2=XL-W1
      WRITE(6,1313)F,D,W1,W2
 1313 FORMAT(1H1,' FREQUENCY=',E10.3,'HZ   SLAB THICKNESS=',F8.4  ,'INCH
     1   W1=',F8.4,5X,'W2=',F8.4)
      WRITE(6,8888)XLT
 8888 FORMAT(' LOSS TANGENT=',E15.8/)
      WRITE(6,1444)
 1444 FORMAT(' PHD    - ASPECT ANGLE IN DEGREES'/' DBHTT - TOTAL RADIATIO
     1N FIELD IN DB'//)
      B=2.0*PI*F/3.0E08
      ESO = 8.85E-12
      T = 2.54E-2
      W1=W1*T
      W2=W2*T
```

```
      D=D*T
      V1=V1*T
      V = (FSR-1.0)*(B**2)*(D**2)
      CALL SHP(F,FSR,D,V,FSIL,BETA,U,IER)
      XD=FSIL*D
      AA=FSR*FSO
      P=XLT*AA
      EL=CMPLX(AA,-P)
      CALL HSP(D,F,EL,XD,Z,IER)
      ZK=((2.*PI*F)**2)*4.*PI*1.E-7*EL
      CBETA=CSQRT(ZK-(Z*Z/(D**2)))
      CU=CSQRT(ZK-B*B-(Z*Z/(D**2)))
      CESIL =Z/D
      CESR=EL/FSO
      CBETA=CONJG(CBETA)
      CU=CONJG(CU)
      CESIL=CONJG(CESIL)
      CESR=CONJG(CESR)
      CALL HTS(D,CU,B,TS,IER)
C C2 IS THE REFLECTION COEFFICIENT
      C2=-CCOS((TS+PI)/3.)/CCOS((TS-PI)/3.)
      I=0
      PHD =-1.0
    1 PHD = PHD + 2.0
      PH = PHD*0.01745
      I=I+1
      X=B*CSQRT(CESR-COS(PH)*COS(PH))*D
      HGO=-2.*PI*F*CESR*FSO*SIN(PH)*CEXP(CMPLX(.0,-PI/4.))/((CESR*SIN(PH
     1)*CCOS(X)-CMPLX(.0,1.)*CSQRT(CESR-COS(PH)*COS(PH))*CSIN(X))*
     1SQRT(2.*PI*B))
      CSW=-2.*PI*F*CESR*CESR*FSO*CU*CU*CESIL/(CBETA*CSIN(CESIL*D)*(CESR*
     1(ZK-B*B)+CU*D*(CU*CU*CESR*CESR+CESIL*CESIL)))
      CCSW1=CSW*CEXP(CMPLX(.0, 1.)*CBETA*W1)
      CCSW2=CSW*CEXP(CMPLX(.0, 1.)*CBETA*W2)
      CI1=2.*CEXP(CMPLX(.0,-PI/6.))*CSIN(TS/3.)/(B*SIN(PI/3.)*CSIN(TS))
      CI2=2.*CEXP(CMPLX(.0,-PI/3.))*CSIN(2.*TS/3.)/(B*SIN(2.*PI/3.)*
     1CSIN(TS))
      C1=CSQRT(B*B+CU*CU)
      A=CMPLX(.0,-4.)*C1/(CMPLX(.0,3.)*C1*CI1-SQRT(3.)*(CI1*CU-CI2*B*
     1CEXP(CMPLX(.0,2.*PI/3.))))
      HD=A*SQRT(2./(PI*B))*CEXP(CMPLX(.0,-5.*PI/12.))/(-CU-CMPLX(.0,B)*
     1SIN(PH))
      E1=B*W1
      E2=B*W2
      IF(PHD.LT.180.)GO TO 4441
      DH=(PHD-360.)*.01745
      GO TO 4442
 4441 DH=PH
 4442 HD1 =CCSW1*HD*COS((PI/2.0+DH)/3.0)*CEXP(CMPLX(0.0,-E1*COS(PH)))
      HD2 =CCSW2*HD*COS((3.0*PI/2.0-PH)/3.0)*CEXP(CMPLX(0.0,E2*COS(PH)))
      XN=1.5
7     XLMDA=3.0E08/F
      DD=A*SQRT(2./(PI*B))*CEXP(CMPLX(.0,-5.*PI/12.))/(-CU+CMPLX(.0,B))
6     HD10=CCSW1*DD
      HD20=CCSW2*DD
5     IF(PHD.LT.90.)GO TO 661
      PHV=450.-PHD
4     GO TO 662
  661 PHV=90.-PHD
3 662 PHV=-90.+PHD
      YVD=(D+V1)/XLMDA
2     CALL DERCF(DVDR,XN,YVD,PHV,XLMDA)
```

```
      CALL DERCF(DVDL,XW,YW,PHW,XL,DA)
      DVDR=CONJG(DVDR)
      DVDL=CONJG(DVDL)
      HD11=HD10*DVDR*CEXP(CMPLX(0.0,+B*(()+V1)*(1.0+SIN(PH))-U1*COS(PH))
     1))/SQRT(D+V1)
      HD21=HD20*DVDL*CEXP(CMPLX(0.0, B*(()+V1)*(1.0+SIN(PH))+U2*COS(PH))
     1))/SQRT(V1+D)
C THIS SUBROUTINE COMPUTES THE SLAB RADIATION FIELD
      PHF=PHD+90.0
      W=2.0*W1
      CALL HSLAB (D,V1,F,W,CESR,CU,CBETA,CESIL,CCSW1,PHF,HYF)
      HYF=HYF*CEXP(CMPLX(0.0,-B*U1*COS(PH)))
      PHB=270.0-PHD
      W=2.0*W2
      CALL HSLAB (D,V1,F,W,CESR,CU,CBETA,CESIL,CCSW2,PHB,HYB)
      HYB=HYB*CEXP(CMPLX(0.0,B*U2*COS(PH)))
      HY=HYF+HYB
      HY = HY*(1.0-C2)
      IF(PHD.LT.90.0)GO TO 2221
      IF(PHD.LT.180.0)GO TO 2222
      IF(PHD.LT.270.0)GO TO 2223
      HT=HD1+HD11+HD21
      GO TO 2224
2221. HT=HGO+HD1+HD2+HD11
      GO TO 2224
2222  HT=HGO+HD1+HD2+HD21
      GO TO 2224
2223  HT=HD2+HD21+HD11
2224  HTT=HT+HY
      AHT=CABS(HT)
      AHTT = CABS(HTT)
      DBHT=20.*ALOG10(AHT)
      DBHTT = 20.0*ALOG10(AHTT)
      AUH(I)=DBHT
      AUHS(I)=DBHTT
      IF(PHD.LT.359.0)GO TO 1
      FN1=(AUHS(45)+AUHS(46))/2.
      Y2=FN-FN1
      ANGLE=-1.
      DO3333 I=1,180
      ANGLE=ANGLE+2.0
      DBHT=AUH(I)+Y2
      DBHTT=AUHS(I)+Y2
      WRITE(6,444)ANGLE,DBHT,DBHTT
  444 FORMAT(' PHD=',F9.2,2X, 'DBHT=',F10.3,2X,'DBHTT=',F10.3)
 3333 CONTINUE
      GO TO 1212
 1112 STOP
      END
      SUBROUTINE HTS(U,CU,B,TS,IER)
      COMPLEX CU,TS,TSO,TSI,DCU,TSR
7     CY=U/B
      CALL THET(CY,CI)
6     TSO=CMPLX(3.141592/2.,-CI)
      DEL=1.E-5
5     A=AIMAG(CU)/REAL(CU)
      AA=ABS(A)
4     TSI=TSO
      IF(AA.LE.DEL)GO TO 10
3     1  DCU=CMPLX(REAL(CU),REAL(CU)*A*DEL/AA)
      CALL CRTS(DCU,B,TSI,TSR,IER)
2     IF(IER.EQ.1)GO TO 3
```

```
      TSI=TSR
      DEL=DEL+1.E-5
      IF(AA.GT.DEL)GO TO 1
   10 CALL CRTS(CU,B,TSI,TS,IER)
    3 RETURN
      END
      SUBROUTINE CRTS(CU,B,TSO,TS,IER)
      COMPLEX F,CU,TS,DTSO,TSI,DTSI,TC,TSO
      F(CU,B,TC)=(CSQRT(1.+CU*CU/(B*B))-CSIN(TC))/CCOS(TC)
      N=0
      DTSO=F(CU,B,TSO)
      T1=CABS(DTSO)
      TSI=TSO+DTSO
    1 A=CABS(CSQRT(1.+CU*CU/(B*B))-CSIN(TSI))
      DTSI=F(CU,B,TSI)
      T2=CABS(DTSI)
      IF(A.LT.1.D-5)GO TO 2
      IF(T2.GT.T1)GO TO 3
      T1=T2
      TSI=TSI+DTSI
      N=N+1
      IF(N.GE.30)GO TO 5
      GO TO 1
    2 IER=0
      TS=TSI
      GO TO 7
    3 IER=1
      WRITE(6,4)
    4 FORMAT(' THIS ITERATION DOES NOT CONVERGE')
      GO TO 7
    5 IER=1
      WRITE(6,6)
    6 FORMAT(' THIS COMPUTATION DOES NOT CONVERGE IN 30 ITERATIONS')
    7 RETURN
      END
      SUBROUTINE HSWP(D,F,EL,XO,Z,IER)
      COMPLEX EL,Z,RZ,ZI,ZO,EP
      ZO=CMPLX(XO,.0)
      DEL=1.E-5
      AIEL=AIMAG(EL)
      REL=REAL(EL)
      A=ABS(AIEL)/REL
      ZI=ZO
      IF(A.LE.DEL)GO TO 10
    1 EP=CMPLX(REL,-REL*DEL)
      CALL CRSWP(D,F,EP,ZI,RZ,IER)
      IF(IER.EQ.1)GO TO 3
      ZI=RZ
      DEL=DEL+1.E-5
      IF(A.GT.DEL)GO TO 1
   10 CALL CRSWP(D,F,EL,ZI,Z,IER)
    3 RETURN
      END
      SUBROUTINE CRSWP(D,H,EL,ZO,RZ,IER)
      COMPLEX ZO,RZ,EL,Z,F,G,FP,GP,DZO,DFG,ZI,DZI,ZK,E1,ZZ
      F(Z)=Z*CSIN(Z)
      G(EL,ESO,ZK,B,D,Z)=EL*CSQRT((ZK-B*B)*D*D-Z*Z)*CCOS(Z)/ESO
      FP(Z)=Z*CCOS(Z)+CSIN(Z)
      GP(EL,ESO,ZK,B,D,Z)=-(EL/ESO)* (Z*CCOS(Z)+((ZK-B*B)*D*D-Z*Z)*
     1CSIN(Z))/CSQRT((ZK-B*B)*D*D-Z*Z)
      ESO=8.85E-12
      PI=3.14159
```

```
      B=2.*PI*H/3.E08
      ZK=((2.*PI*H)**2)*4.*PI*1.E-7*EL
      N=0
      DZO=-(F(ZO)-G(EL,ESO,ZK,B,O,ZO))/(FP(ZO)-GP(EL,ESO,ZK,B,O,ZO))
      T1=CABS(DZO)
      ZI=ZO+DZO
    1 DFG=F(ZI)-G(EL,ESO,ZK,B,O,ZI)
      A=CABS(DFG)
      DZI=-(F(ZI)-G(EL,ESO,ZK,B,O,ZI))/(FP(ZI)-GP(EL,ESO,ZK,B,O,ZI))
      T2=CABS(DZI)
      IF(A.LT.1.E-5)GO TO 2
      IF(T2.GT.T1)GO TO 3
      T1=T2
      ZI=ZI+DZI
      N=N+1
      IF(N.GE.30)GO TO 5
      GO TO 1
    2 IER=0
      RZ=ZI
      GO TO 7
    3 IER=1
      WRITE(6,4)
    4 FORMAT(' THIS ITERATION DOES NOT CONVERGE IN SEARCHING FOR COMPLEX
     1 ROOT OF SURFACE WAVE POLE')
      GO TO 7
    5 IER=1
      WRITE(6,6)
    6 FORMAT(' THIS COMPUTATION DOES NOT CONVERGE IN 30 ITERATIONS IN SE
     1ARCHING FOR COMPLEX ROOT OF SURFACE WAVE POLE')
    7 RETURN
      END
      SUBROUTINE SWP(Z,ESR,D,V,ESIL,BETA,U,IER)
C     THIS ROUTINE IS TO FIND THE ROOT OF THE POLE OF SURFACE WAVE BY
C     USING THE BISECTION METHOD. BE SURE TO CHECK THE FIRST TWO
C     APPROXIMATIONS X1 AND X2 SUCH  THAT F(X1)*F(X2) IS NEGATIVE
      F(X) = TAN(X) - ESR *SQRT((V/(X*X))-1.0)
      B=2.0*3.14159*Z/3.0E08
      BK=SQRT(ESR)*B
      IF(D.LT.2.54E-5)GO TO 1000
      N = 0
      X1=SQRT(V)*1.E-4
      TV=1.5708
      SV=SQRT(V)
      IF(SV.GE.TV)GO TO 1111
      X2=SQRT(V)*.9999
      GO TO 992
 1111 X2=TV-0.0001
  992 Y1=F(X1)
      Y2 = F(X2)
    1 X = (X1+X2)/2.0
      N = N + 1
      IF (N.GT.30) GO TO 2
      IF(F(X1)*F(X))100,101,102
  100 X2 = X
      IF((X2-X1).LT.1.0E-5) GO TO 101
      GO TO 1
  102 X1 = X
      IF((X2-X1).LT.1.0E-5) GO TO 101
      GO TO 1
  101 ESIL=X/D
      BETA = SQRT(BK**2-ESIL**2)
      U = SQRT(BETA**2-B**2)
```

```
      GO TO 1001
 1000 U=(ESR-1.0)*B*B*0/ESR
      BETA=SQRT(U*PI+B*B)
      ESIL=B*SQRT(ESR-1.0)
 1001 IER=0
      GO TO 3
    2 IER = 1
      PRINT4
    4 FORMAT(' ','FAILED TO CONVERGE IN 30 ITERATIONS IN SEARCHING FOR
     1THE ROOT OF THE POLE OF SURFACE WAVE')
    3 RETURN
      END
      SUBROUTINE THET(P,C)
C     THIS ROUTINE IS TO COMPUTE A CONSTANT BY FINDING A ROOT OF A
C     POLYNOMIAL BY USING THE SECAND METHOD IN ORDER TO COMPUTE THE
C     CHU-KOUYOUMJIAN'S COEFFICIENT
      F(X) = SINH(X)-P
      X = 0.0
      X1 = P
      Y = F(X)
      Y1 = F(X1)
      DO 1 I = 2,20
      X2 = (X*F(X1)-X1*F(X))/(F(X1)-F(X))
      Y = F(X2)
      IF(ABS(X2-X1).LT.1.E-5) GO TO 2
      X = X1
    1 X1 = X2
      WRITE(6,6)
    6 FORMAT(/36HOFAILED TO CONVERGE IN 20 ITERATIONS)
      GO TO 3
    2 C = X2
    3 RETURN
      END
      SUBROUTINE DERCF(D,XN,Y,B,XLMDA)
C     THIS ROUTINE IS TO COMPUTE THE DIFFRACTION COEFFICIENT
      COMPLEX F1J,F2J,Q,R,T1,D1,T2,D2,D,F1,F2,S
      PI=3.1415927
      BR=B*0.01745329
      ARG1=(PI+BR)/(2.0*XN)
      ARG2=(PI-BR)/(2.0*XN)
      CX1=COS(ARG1)
      CX2=COS(ARG2)
      SX1=SIN(ARG1)
      SX2=SIN(ARG2)
      X1=(BR+PI)/(2.0*XN*PI)
      N1=X1
      E1=X1-N1
      IF(E1.GT.0.5) N1=N1+1
      IF(E1.LT.-0.5) N1=N1-1
      FN1=FLOAT(N1)
      X2=(BR-PI)/(2.0*XN*PI)
      N2=X2
      E2=X2-N2
      IF(E2.GT.0.5) N2=N2+1
      IF(E2.LT.-0.5) N2=N2-1
      FN2=FLOAT(N2)
      A1=1.0+COS(-BR+2.0*XN*PI*FN1)
      A2=1.0+COS(-BR+2.0*XN*PI*FN2)
      SA1=SQRT(A1)
      SA2=SQRT(A2)
      XX=(SQRT(2.0*PI*Y))*SA1
      YY=(SQRT(2.0*PI*Y))*SA2
```

```
      XXS=XX*XX
      YYS=YY*YY
      PO=SQRT(PI/2.0)
      CALL CS(C1,S1,XXS)
      CC1=0.5-C1
      SS1=0.5-S1
      F1J= PO*CMPLX(SS1,CC1)
      CALL CS(C2,S2,YYS)
      CC2=0.5-C2
      SS2=0.5-S2
      F2J= PO*CMPLX(SS2,CC2)
      P=-PI/4.0
      Q=CMPLX(0.0,P)
      R=CEXP(Q)
      S=(-0.25*R*SQRT(XLMDA))/(PI*XN)
      T1=S*2.0*CEXP(CMPLX(0.0,XXS))
      D1=T1*F1J*CX1*(XX/SX1)
      T2=S*2.0*CEXP(CMPLX(0.0,YYS))
      D2=T2*F2J*CX2*(YY/SX2)
      D= D1+D2
      RETURN
      END
      SUBROUTINE HSLAB (D,V1,F,W,CESR,CU,CBETA,CESIL,CCSW,PHD,HT)
C     THIS ROUTINE IS TO COMPUTE THE SLAB RADIATION FIELD
      COMPLEX CCSW,HY1,HT,CESR,CU,CBETA,CESIL,XKX,XKXD,ZK
      PI = 3.14159
      ESO = 8.85E-12
      XLMDA=3.0E08/F
      B=2.0*PI/XLMDA
      ZK=CESR*B*B
      XKX=CSQRT(ZK-CBETA*CBETA)
      XKXD=XKX*D
      HT=CMPLX(0.0,0.0)
      IM=D/(0.05*XLMDA)
      DO 222 I = 1,IM
      M=2*I-1
      DI=D*M/(2.*IM)
      CALL CASER(D,F,W,V1,CESR,CU,CBETA,CESIL,XLMDA,DI,PHD,HY1)
      HT=HT+HY1*CCOS(XKX*(D-DI))
  222 CONTINUE
      HT=CONJG(HT)
      HT=HT*D*CMPLX(.0,-1.)*CBETA*CCSW/(IM*CCOS(XKXD))
      RETURN
      END
      SUBROUTINE CASER(D,F,W,V1,CESR,CU,CBETA,CESIL,XLMDA,DI,PHD,H)
      COMPLEX DH1,DHY,DH2,H,HY,HD1,HD2,FG,GB,CESR,CU,CBETA,CESIL,UK
      COMPLEX C
      PI=3.14159
      BK=2.0*PI/XLMDA
      IF(PHD .GT. 270.)PHD=PHD-360.
      PH=PHD*.01745
7     UK=CU/BK
      ARG=BK*DI
6     CALL GREENF(PHD,ARG,UK,XLMDA,FG)
      HY=FG
5     C=CEXP(CMPLX(.0,-PI/4.))/SQRT(2.*PI*BK)
      XN=1.5
4     Y=(D+V1)-DI
      YD=Y/XLMDA
3     PH1=180.0-PHD
      CALL DERCF(DH1,XN,YD,PH1,XLMDA)
2     HD1=C*DH1*CEXP(CMPLX(0.0,(BK*(D+V1)*COS(PH)-BK*Y)))/SQRT(Y)
```

```
      CALL DERCF(DHY,XN,YD,0.0,XLMDA)
      Y2=(D+V1)/XLMDA
      CALL DERCF(DH2,XN,Y2,PHD,XLMDA)
      HD2=C*DHY*DH2*CEXP(CMPLX(.0,(-BK*(D+V1)-BK*Y)))/SQRT(Y*(D+V1))
      IF(PHD.LT.0.)GO TO 1113
      IF(PHD.LT.180.) GO TO 1111
      H=HY+HD2
      GO TO 2
 1113 H=HD1
      GO TO 2
 1111 H=HY+HD1+HD2
 2    CONTINUE
      RETURN
      END
      SUBROUTINE GREENF(PHD,ARG,UK,XLMDA,F)
      COMMON BJ(150),BY(150)
      COMPLEX F,N,NM,G,GM,P,UK ,AI
      P(X)=CEXP(CMPLX(.0,X))
      PI=3.141592
      PH=PHD*PI/180.
      B=2.*PI/XLMDA
      XN=1.5
      AI=CMPLX(.0,1.)
      N=(.0,.0)
      DO 5 M=1,20
      I=M-1
      EM=2.
      IF(I .EQ. 0)EM=1.
      BM=BESSJ(ARG,I/XN,BJ,BY,IER)
      NM=EM*BM*P(I*PI/(2.*XN))*COS(I*PH/XN)
      N=N+NM
      ANM=CABS(NM)
      IF(ANM .LT. 1.E-30)GO TO 44
 5    CONTINUE
 44   G=(.0,.0)
      DO 15 M=1,20
      I=M-1
      BM=BESSJ(ARG,(2.*I+1.)/(2.*XN),BJ,BY,IER)
      GM=BM*P((2.*I+1.)/(4.*XN))*COS((2.*I+1.)*PH/(2.*XN))
      G=G+GM
      AGM=CABS(GM)
      IF(AGM .LT. 1.E-30)GO TO 55
 15   CONTINUE
 55   C=SQRT(2./(PI*B))/XN
      G=G*C*P(-PI/4.)
      N=N*C*P(-PI/4.)/2.
      RU=REAL(UK)
      AIU=AIMAG(UK)
      IF((PHD .EQ. 90.) .OR. (PHD .EQ. 270.))GO TO 11
      IF((RU .EQ. 0.) .AND. (AIU .EQ. 0.))GO TO 22
      F=(AI*COS(PH)*N+UK*G)/(AI*COS(PH)+UK)
      GO TO 33
 11   F=G
      GO TO 33
 22   F=N
 33   RETURN
      END
```


U.S. GOVERNMENT PRINTING OFFICE: 1974-737-726/89 REGION NO. 3-11

NATIONAL AERONAUTICS AND SPACE ADMINISTRATION
WASHINGTON, D.C. 20546

OFFICIAL BUSINESS
PENALTY FOR PRIVATE USE $300

SPECIAL FOURTH-CLASS RATE BOOK

POSTAGE AND FEES PAID
NATIONAL AERONAUTICS AND SPACE ADMINISTRATION
451

U.S.MAIL

POSTMASTER: If Undeliverable (Section 158 Postal Manual) Do Not Return

"The aeronautical and space activities of the United States shall be conducted so as to contribute . . . to the expansion of human knowledge of phenomena in the atmosphere and space. The Administration shall provide for the widest practicable and appropriate dissemination of information concerning its activities and the results thereof."

—NATIONAL AERONAUTICS AND SPACE ACT OF 1958

NASA SCIENTIFIC AND TECHNICAL PUBLICATIONS

TECHNICAL REPORTS: Scientific and technical information considered important, complete, and a lasting contribution to existing knowledge.

TECHNICAL NOTES: Information less broad in scope but nevertheless of importance as a contribution to existing knowledge.

TECHNICAL MEMORANDUMS: Information receiving limited distribution because of preliminary data, security classification, or other reasons. Also includes conference proceedings with either limited or unlimited distribution.

CONTRACTOR REPORTS: Scientific and technical information generated under a NASA contract or grant and considered an important contribution to existing knowledge.

TECHNICAL TRANSLATIONS: Information published in a foreign language considered to merit NASA distribution in English.

SPECIAL PUBLICATIONS: Information derived from or of value to NASA activities. Publications include final reports of major projects, monographs, data compilations, handbooks, sourcebooks, and special bibliographies.

TECHNOLOGY UTILIZATION PUBLICATIONS: Information on technology used by NASA that may be of particular interest in commercial and other non-aerospace applications. Publications include Tech Briefs, Technology Utilization Reports and Technology Surveys.

Details on the availability of these publications may be obtained from:

SCIENTIFIC AND TECHNICAL INFORMATION OFFICE

NATIONAL AERONAUTICS AND SPACE ADMINISTRATION

Washington, D.C. 20546